



Article

# Characterization of UV Light Curable Piezoelectric 0-0-3 Composites Filled with Lead-Free Ceramics and Conductive Nanoparticles

Rytis Mitkus \*, Lena Piechowiak and Michael Sinapius

Institute of Mechanics and Adaptronics, Technische Universität Braunschweig, Langer Kamp 6, 38106 Braunschweig, Germany

\* Correspondence: r.mitkus@tu-braunschweig.de or mitkus.rytis@gmail.com

**Abstract:** Lead-free piezoelectric materials are essential for our healthy future but offer lower performance than lead-based materials. Different material combinations are explored to improve the performance of lead-free materials. By filling the UV light curable photopolymer resin with 30 vol.% lead-free piezoelectric ceramics and with up to 0.4 wt.% conductive nanofillers, thin and flexible piezoelectric 0-0-3 composites are formed. Two particle sizes of Potassium Sodium Niobate (KNN) and Barium Titanate (BTO) ceramics were used with four conductive nanofillers: Graphene Nanoplatelets (GNPs), Multi-Walled Carbon Nanotubes (MWCNTs), and two types of Graphene Oxide (GO). Resulting high viscosity suspensions are tape-cast in a mold as thin layers and subsequently exposing them to UV light, piezoelectric composite sensors are formed in 80 s. Even low nanofiller concentrations increase relative permittivities, however, they strongly reduce curing depth and increase undesirable dielectric losses. Non-homogeneous dispersion of nanofillers is observed. In total, 36 different compositions were mixed and characterized. Only six selected material compositions were investigated further by measuring mechanical, dielectric, and piezoelectric properties. Results show KNN composite performance as piezoelectric sensors is almost six times higher than BTO composite performance.



**Citation:** Mitkus, R.; Piechowiak, L.; Sinapius, M. Characterization of UV Light Curable Piezoelectric 0-0-3 Composites Filled with Lead-Free Ceramics and Conductive Nanoparticles. *J. Compos. Sci.* **2023**, *7*, 89. <https://doi.org/10.3390/jcs7020089>

Academic Editor: Stelios K. Georgantzinos

Received: 27 January 2023

Revised: 7 February 2023

Accepted: 15 February 2023

Published: 20 February 2023



**Copyright:** © 2023 by the authors. Licensee MDPI, Basel, Switzerland. This article is an open access article distributed under the terms and conditions of the Creative Commons Attribution (CC BY) license (<https://creativecommons.org/licenses/by/4.0/>).

## 1. Introduction

Two-phase piezoelectric composites have been researched extensively for several decades [1–8]. They are an alternative to bulk piezoelectric ceramic sensors, which are brittle [4,9], possess poorer manufacturability [2,9,10] and can have only basic geometries. Piezoelectric composites are flexible, their properties such as mechanical strength, density, and acoustical impedance can be tailored to the application [9–11], making them suitable for Structural Health Monitoring (SHM) applications [12].

The piezoelectric properties of 2-phase composites, without any particle modifications or other material additions, are low because of the low relative permittivity and conductivity of the passive polymer phase [1,9–11,13,14], which complicates poling [15]. Furthermore, such composites are usually made with Lead zirconate titanate (PZT) that has high lead content (≈60 wt.%) [16], which causes concerns during PZT processing where the vapor of lead is released in the atmosphere [17,18].

Interest was shown in composites based on Barium Titanate (BTO) and/or Potassium Sodium Niobate (KNN) piezoelectric ceramics [4,19–25]. PZT substitution with the lead-free piezoelectric ceramics, such as BTO and KNN [26], which show lower piezoelectric properties compared to PZT [27–30], produces the lower piezoelectric performance of

the composite materials but eliminates any possible environmental and health problems associated with lead vapor release into the atmosphere.

From many possible approaches to increase the performance of 2-phase composites, the addition of small amounts of conductive carbon-based nanofillers to the material mixture increases the relative permittivity and conductivity of the polymer matrix [1,15,31–33] and therefore, poling efficiency of the piezoelectric composites is improved, which results in an improved piezoelectric performance [15,34,35]. The addition of conductive nanofillers forms so-called piezoelectric 0-0-3 composites. Previous studies used various types of conductive nanofillers in polymer-based composites to improve their dielectric properties, e.g., Graphene Oxide (GO) [36], Graphene [19,37], Graphene nanoplatelets (GNPs) [38,39], Carbon Nanotubes (CNTs) [40,41], or metal particles [42–44].

These nanofillers possess high conductivity, large aspect ratio, and high mechanical properties [31,40,43]. While GO does not possess high electric properties [45], after reduction, e.g., by UV light, the electrical properties of reduced GO (rGO) increase [46,47]. GO can be also easily dispersed in organic solvents [45,46], helping to ensure good nanofiller dispersion in the composites. Using carbon-based nanofillers at very low amounts can lead to a great enhancement of piezoelectric and mechanical properties of the composites [3,46,48–52].

This study aims to find which piezoelectric composite material compositions produce the highest piezoelectric performance. Few studies examined 0-0-3 composites with lead-free BTO ceramics, and none were found using KNN. Therefore, this knowledge gap is investigated in this study. Two types of ceramics (fixed at 30 vol.%), each containing two different particle sizes, are dispersed with four different types of conductive carbon-based nanomaterials (between 0 and 0.4 wt.%) in UV light curable photopolymer resin. The resulting suspensions, after manual tape-casting and solidification under UV light, form the desired geometry piezoelectric composites (square), which were poled, characterized, and their piezoelectric performance was measured.

### 1.1. Nanofillers in Composites

Nanofillers mostly tend to form agglomerates and are difficult to disperse homogeneously in a polymer matrix [45,53] due to high surface area to volume ratio and resulting high surface energy [54]. There is also considerable disagreement regarding the effect of nanofiller agglomerations on the properties of the composite. Some studies found an improved ability of small agglomerates to form electrical paths [55,56], others found a uniform distribution to be beneficial [57–59]. However, agglomerates cause higher stresses in the composites and can lead to lower mechanical strength [55,60], while at the same time, agglomerates of conductive nanofillers might have local conductive areas making poling of the composites impossible. Therefore, the homogeneous dispersion of nanofillers should be prioritized for piezoelectric composites.

Established dispersion methods for nanofillers are three-roll milling and ultrasonication [58,61]. However, both techniques may result in the breakage of nanofillers, especially CNTs [58,61]. Yet, ultrasonication is still the superior method to disperse nanofillers in polymer suspensions [62], but requires the addition of solvent and subsequent dispersion [63,64]. Our previous experiments showed that an ultrasonic bath was insufficient for achieving a homogeneous dispersion [57] and ultrasonication with an ultrasonic sonotrode produces more homogeneous particle dispersion. When using ultrasonication, after the dispersion of all particles and polymer in the solvent, the solvent is evaporated leaving a highly viscous suspension [63,64].

### 1.2. Composite Manufacturing with UV Light

Different manufacturing methods for piezoelectric composites have been reported in the literature. Generally, a distinction between subtractive, forming, and additive processes can be drawn [13,65–68]. The major drawback of using either subtractive or forming methods to manufacture piezoelectric composites is its difficulty to implement, leading to high

production times, high costs, and limited geometries [67,69]. UV light-based piezoelectric composite material solidification provides many advantages over the above-mentioned methods, such as reduced material waste, fast manufacturing, and geometrical freedom. UV light curable composites, where piezoelectric ceramic particles are embedded in a liquid photopolymer resin phase, which solidifies under the UV light [70], can also be used in Additive Manufacturing (AM) techniques such as Stereolithography (SLA) [71] or Direct Light Projection (DLP) [66–69,72–81]. The DLP process solidifies the complete layer at once [81], which helps to reduce manufacturing times and lowers costs [72–74]. Even if commercially available AM systems are not suitable/capable to solidify the composites because of the low-power UV light sources used, single-layer tape-casting methods in a shape/mold still provide additional geometrical freedom, waste reduction, decrease in manufacturing time and costs than subtractive or forming methods [69,82]. The use of UV light curable photopolymers for piezoelectric composite manufacturing allows an optimization of the sensor geometry which can further enhance piezoelectric properties [66,68,80] and even improve sensor response by adapting sensor geometry to SHM applications [83,84]. Therefore, further development of UV light curable piezoelectric composites is of high interest.

When using UV light curable photopolymers to manufacture piezoelectric composites, the main problem is low curing depths. Solid particles (both ceramic and nanofillers) absorb, block, and scatter UV light and result in a reduction in curing depth and printing accuracy [55,73,76,81]. Piezoelectric ceramic particle size [85], connectivity [40,86], and volume fraction of the ceramics influence the properties of the piezoelectric composites [86]. Increasing the volume fraction of the ceramic is necessary for the highest piezoelectric performance but it decreases mechanical properties, especially the flexibility of the composites [31,32], and also decreases curing depth. A reduction in piezoelectric particle size (while keeping ceramic particle loading constant) increases scattering of the UV light as particle surface area increases and strongly reduces curing depth [73,87]. Bigger ceramic particles are overall more suitable for the addition to the photopolymers because of a lower reduction in curing depth [75,88,89], easier dispersion, and formation of fewer voids. Another problem is the difference in refractive index between the embedded particles and photopolymer resin, which further decreases curing depth [88–90]. To achieve higher curing depths, the intensity of the UV light source, exposure time, or photoinitiator content can be increased, or a combination of the methods proposed [87,89,91], but this might also result in increased curing width, which in turn could reduce resolution if a 3D printing process is used to achieve complex geometries.

## 2. Materials and Methods

The detailed extension of this chapter can be found in the Supplementary Materials.

### 2.1. Materials

In total, two different lead-free piezoelectric ceramics, Barium Titanate (BTO) (purchased from Nanografi Nanotechnology AS, Çankaya/Ankara, Turkey) and Sodium Potassium Niobate (KNN) (purchased from Nippon Chemical Industrial Co., Ltd., Tokyo, Japan) are investigated in this study. Two particle sizes of each ceramic are available, therefore, in total four piezoelectric ceramics are investigated. Ceramic materials are further named BTO7, BTO13, KNN3, and KNN6 with respect to their mean particle sizes. Scanning Electron Microscopy (SEM) images of the ceramics as received (Figure S1) and X-ray Diffraction (XRD) data of the ceramics as received (Figure S2) can be found in the Supplementary Materials.

The XRD patterns (Figure S2) compared to the literature suggest orthorhombic and orthorhombic/tetragonal lattice structures of KNN6 and KNN3, respectively [92–96]. XRD data of BTO suggests that both BTO materials used in this study have a tetragonal lattice structure [97–100]. Detailed XRD pattern evaluation is in Supplementary Materials.

The properties of the ceramics are listed in Table S1. Refractive indexes, piezoelectric charge coefficients  $d_{33}$ , relative permittivities, dielectric losses, and coercive fields of ce-

amics were not measured in this study and are taken from the literature. Ceramic content in the piezoelectric composites investigated in this study was always kept constant at 30 vol. %.

From SEM images of ceramics (Figure S1), both BTO ceramics show oval/spherical particle geometry, while some particles have sharp edges. KNN3 ceramic particles show irregular geometry, particles are partially sintered together. On the other hand, KNN6 has a rectangular particle geometry with a few particles only showing irregular geometries. All four ceramic particle size distribution is between 30–40%.

Four types of different conductive nanofillers are used in this study: COOH (carboxylic acid)—functionalized Multi-Walled Carbon nanotubes (MWCNTs) (purchased from FutureCarbon GmbH, Bayreuth, Germany), Graphene Nanoplatelets (GNPs) (purchased from IoLiTec-Ionic Liquids Technologies GmbH, Heilbronn, Germany), Graphene oxide (GO<sub>2</sub>) and Graphene oxide (GO<sub>3</sub>) (both graphene oxides purchased from The Sixth Element (Changzhou) Materials Technology Co., Ltd., Jiangsu, China). All materials have been used as received without further modifications. The SEM images of nanomaterials (Figures S3–S6) and properties (Table S2) can be found in the Supplementary Materials.

Graphene was shown to absorb UV light in the range of 100 to 320 nm wavelength with its peak at 280 nm, however, the light is scattered at lower and higher wavelengths [101]. MWCNTs absorb light up to wavelengths of 380 nm with its peak at 312 nm [48,101]. However, UV light absorption/scattering also depends on nanofiller dispersion [101] and concentration, where better dispersion and higher concentrations decrease curing depth. Therefore, different results with the use of every nanofiller are expected.

MWCNTs used in this study show similarities to the morphology of MWCNTs reported in literature [56]. GNPs seem to have particle-like geometry (Figure S4) and form huge agglomerations of diameters up to 50 µm, but without the flaky structure which is known for GNPs from literature [55,102] and are considered fragmented. High loadings of this type of GNPs are necessary to improve composite properties. On the other hand, both GO materials used in this study look lamellar, consisting of multiple creased thin layers stacked together, similar to reports in the literature [103]. Comparing GO<sub>2</sub> and GO<sub>3</sub> used in this study, GO<sub>3</sub> takes twice as high volume for the same amount of GO<sub>2</sub> because of almost twice as high surface area. As a result of different conductive nanofiller sizes/geometries/types used for composite manufacturing, different characteristics (cure depth, dielectric, mechanical, and piezoelectric properties) for every material composition are expected.

As a matrix material, commercially available photopolymer resin “High-Temperature V2” (Formlabs, Somerville, MA, USA) is used. This photopolymer showed the best performance as matrix material between various types of photopolymers in our previous study [69]. Furthermore, this photopolymer offers high mechanical and thermal properties and is well-suited for piezoelectric composite manufacturing. From the literature, it is known that polymers with higher stiffness can transfer more stress applied to the composite to the ceramic particles and thus increases the performance of piezoelectric composites [66,79,104].

## 2.2. Suspension Preparation and Sensor Manufacturing

All suspensions prepared in this study are dispersed with the same method and parameters: two-step particle dispersion with ultrasonic sonotrode followed by solvent (ethanol (EtOH)) evaporation to form a paste (Figures S7 and S8). Composite suspensions are solidified (cured) under UV light (EQ CL30 LED Flood, Henkel AG & Co. KGaA, Düsseldorf, Germany) for 80 s after tape-casting them manually on the glass (Figures S9 and S10). UV light was applied only from a single side for all composites.

The only exception is the curing cycle for six selected composites for further investigation, where the UV light was applied for 40 s from one side and after short cooling was applied for 40 s from another side to achieve higher homogeneity of the solidified composites. UV light source, with 405 nm wavelength, produces 1.5 W/cm<sup>2</sup> at 50 mm

distance. Peeled composites are washed with acetone and are kept between two glasses for a few days in the dark at room temperature to reduce bending (residual stresses). No additional post-curing with UV light or heat was applied.

After a selection of six composite materials for measurements of piezoelectric properties, a thin, single layer of conductive silver ink (Silberleitlack, type 530042, Ferro GmbH, Remchingen, Germany) is manually applied on both sides of the specimens, leaving 1 mm around the edges uncovered. Electrodes are required for dielectric measurements, poling, and piezoelectric properties measurements. The poling of the specimens took place in Silica oil heated to 55 °C for a total of 21 min (4-min ramp time, 16-min hold time, 1-min ramp-down time). All specimens were poled in a 30 kV/mm electric field.

### 2.3. Characterization Methods

The curing depths of the suspensions are measured over time, using four curing times: 20, 40, 60, and 80 s. SEM is used to investigate as-received ceramic particles, nanofillers, and the cross-sections of broken, solidified piezoelectric composite sensors.

Dielectric measurements in this study include measurements of relative permittivity  $\epsilon_r$  and dielectric loss (dissipation factor  $\tan(\delta)$ ) at 1 kHz at room temperature. Details can be found in the Supplementary Materials. Two types of dielectric measurements were made: without electrodes on the piezoelectric composites and with electrodes. The first method (without electrodes (Figure S11)) was used to measure the dielectric properties of all composites manufactured in this study to roughly compare their dielectric properties. After the manufacturing of all planned material compositions, the specimens of six selected compositions were covered with silver electrodes (described above) and their dielectric properties were remeasured. The dielectric properties of these six selected composites can be compared to the literature.

Young's modulus of the piezoelectric composites was measured for piezoelectric charge coefficient determination with a tensile testing machine. Details can be found in the Supplementary Materials. To characterize and compare the performance of the sensors manufactured in this study, piezoelectric charge coefficients  $d_{31}$  were measured with a 4-point bending setup, adapted and modified from Payo [105]. The method of piezoelectric charge coefficient  $d_{31}$  measurement is described in detail in our previous publication [80] and in Supplementary Materials. It is important to mention that the piezoelectric properties reported in this study are *effective piezoelectric properties* because the sensors were characterized while glued on the substrate. The literature suggests that in such a setup, measured piezoelectric values are approx. 40% lower than by using measuring methods using free-clamped samples [106].

## 3. Results and Discussion: Material Screening

The following presentation and discussion of the results abbreviates the name of the material compositions, namely "30K3" means 30 vol.% of KNN3 piezoelectric ceramic dispersed without nanofillers in the photopolymer matrix and "30B13" means 30 vol.% of BTO13 dispersed without nanofillers in the photopolymer matrix, and so on. On the other hand, materials with nanofillers are named "30K3-0.2GP" for composite containing 30 vol.% of KNN3 and 0.2 wt.% of Graphene Nanoplatelets (GNPs) dispersed in photopolymer matrix. "M" stands for Multi-Walled Carbon Nanotubes (MWCNTs), "GO2" stands for Graphene Oxide 2, and "GO3" stands for Graphene Oxide 3 (see sub-chapter Materials and Methods).

### 3.1. Curing Depth

By measuring the time-dependent curing depths, the influence of the addition of nanofillers on the consolidation of the composite materials can be evaluated. These data help to understand how deep UV light penetrates and is one of the factors helping to decide the suitability of nanofillers for UV light curable piezoelectric composite manufacturing. As high as possible curing depths are desirable. Due to thin specimens and the manual

measuring process, high deviations were observed and the curing depth results present the general change/trend only.

The results of curing depths over UV light exposure time of all prepared compositions are shown in Figure 1. For easier comparison, all graphs have the same Y-axis, except composites without nanofillers (Figure 1A,F), which achieved much higher curing depths. Even the small addition (0.2 wt.%) of any nanofillers drastically decreases the curing depth and makes the solidification of thicker composites difficult. The addition of 0.4 wt.% of nanofillers decreases the curing depth further, but by a smaller degree compared to the influence of 0.2 wt.%. The curing depth increases with increasing curing time for most compositions, as expected, but some compositions already show flattening of the curve, indicating the maximum degree of cure under the conditions used.

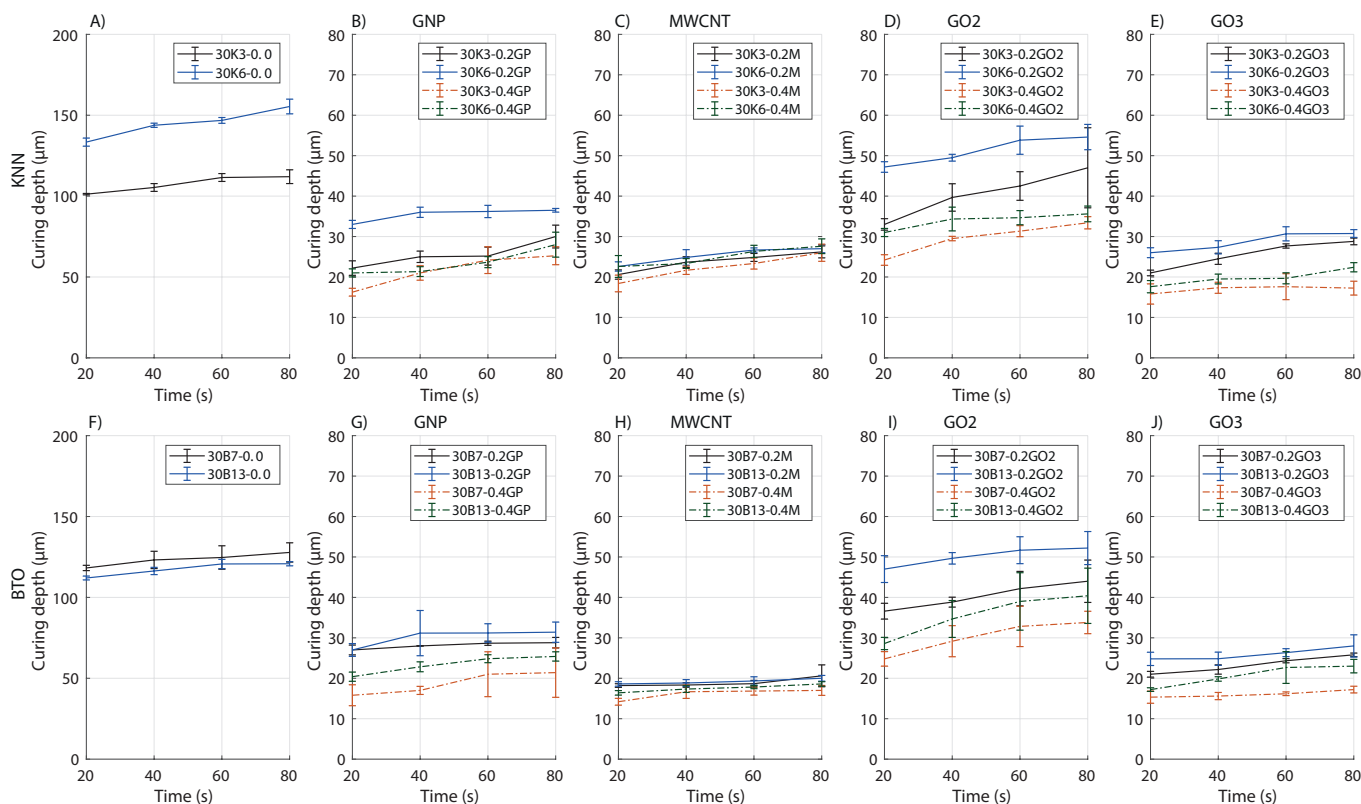


**Figure 1.** Curing depth over curing time of all composites manufactured in the study at room temperature.

The addition of ceramic particles to the photopolymer reduces curing depths because ceramic particles block and scatter UV light [75,89,90]. Curing depth reduction is mainly dependent on ceramic loading (kept constant in this study) and the difference in refractive index between photopolymer and ceramic particles used [50,75,76,87–90,107–109]. Furthermore, most literature reports that smaller ceramic particles reduce curing depth more than the bigger ceramic particles (bigger than the UV light wavelength used) [75,88], while other literature suggests smaller particles, with better light scattering should be preferable [67,79]. It is possible that particle sizes close to the UV light wavelength used (in this study it is 405 nm) might produce the worst results of curing depth because of the highest UV light absorption.

The 30K3 shows the lowest, and 30K6 show the highest curing depth from all two-phase suspension investigated in this study. Both BTO with bigger particles produced almost similar curing depths, and the results fit between 30K3 and 30K6. Low curing depths of BTO are caused by a higher refractive index of BTO ceramic than KNN (Table S1). Since

bigger particles should produce higher curing depths than smaller particles, the results also suggest, that ceramic particles  $>1\text{ }\mu\text{m}$  might not improve curing characteristics.

Interestingly, bigger BTO particles produced slightly lower curing depths than smaller BTO particles. In our previous study, we found that irregular particle geometry with many sharp corners/edges might produce slightly lower cure depths [76], but both BTO ceramic particles are rather spherical. BTO7 has a slightly higher particle size deviation (38.2% for BTO7 and 32.3% for BTO13 (Table S1)) which should decrease curing depth as reported in literature [89], but our findings are the opposite.

The reason why 30B7 produced higher curing depths than 30B13 has not yet been clarified. A possible explanation could be a slightly lower volumetric loading of BTO7 in the suspension since both types of BTO particles were sticking to the walls of the glass jar during solvent evaporation. However, BTO particles were always washed into suspension being evaporated with additional ethanol to minimize the residue of the particles on the walls. Still, some of the BTO7 particles were left on the sides of the glass jar and could have caused lower ceramic loading, which would explain the higher curing depths achieved by the 30B7 composite. This assumption is also supported by BTO suspensions with nanofillers (see Figure 1G–J), where all suspensions with BTO7 and nanofillers produced lower curing depths than the same filled with BTO13.

The results of the suspensions with nanofillers reveal that composites with GO2 show the highest curing depths at all nanofiller loadings, while the suspensions filled with MWCNTs and GO3 show the lowest curing depths. One parameter influencing curing depth is the surface area of the nanofillers (Table S2), however, it does not correlate to the curing depths measured. Another influencing factor is the quality of nanofiller dispersion. GO2 shows the biggest curing depths, especially in suspensions with bigger ceramic particles. They have quite a small surface area ( $285\text{ m}^2/\text{g}$ , see Table S2), blocking less UV light and average particle dispersion (Figures S21–S24). GNP show the second-highest curing depth, and have the highest surface area of all nanofillers investigated here ( $750\text{ m}^2/\text{g}$ ). However, because of extremely poor dispersion (Figures S13–S16), their surface area strongly decreased and high curing depths were achieved. The lowest curing depths are shown by MWCNTs and GO3 suspensions; both show very similar curing depths, but surface areas differ almost five times (Table S2). The MWCNTs are hair-like structures compared to GO3, which are more like platelet-like structures. MWCNTs show many agglomerates, especially in KNN composites, and much better dispersion in BTO composites, which fits the results of curing depth perfectly (see Figure 1C,H) because better dispersion of nanofillers reduces the curing depth more than poor dispersion [57]. On the other hand, GO3 shows good dispersion, has the highest surface area (Table S2), and therefore shows very low curing depths.

To summarize, conductive nanofillers have a significant negative influence on the curing depth, decreasing curing depth up to five times when using MWCNTs and GO3. Low curing depths cause heterogeneous properties over composite thickness, making composite characterization, and the whole composite manufacturing process more difficult. However, to achieve the highest influence on matrix conductivity, good dispersion of nanofillers is a must.

### 3.2. Microstructure

The microstructure of all piezoelectric composites made in this study was investigated with an SEM to investigate ceramic and nanofiller dispersion, and to gain a better understanding of curing. All broken composites used for SEM had UV light exposure for 80 s from the top side only. SEM images are cross-section images after breaking the solidified specimens at room temperature. SEM images of all composites manufactured in this study, at two different magnifications, can be found in Supplementary Materials (Figures S12–S28).

Figure 2 shows the two-phase composites without nanofillers (note different magnifications). The distinct difference between KNN and BTO composites is the solidification

degree of the photopolymer matrix. KNN composites (Figures 2A and S12A) seem to be much stiffer because many particles are missing (see yellow circles in Figure 2). Particles drop during the breaking of the composite. On the other hand, BTO composites (Figures 2B and S12C) show smooth breaks and no missing particles indicating a softer photopolymer matrix. However, looking at the results of curing depth in Figure 1A,F, BTO suspensions show curing depths between KNN3 and KNN6, but SEM images show that both KNN composites have a stiffer matrix (higher degree of cure) than both BTO composites. Therefore, BTO composites should also show rigid matrix and dropped particles. Similar results are visible with almost all BTO composites prepared in this study. The only feasible explanation is the higher refractive index of BTO particles (Table S1), which causes such a low degree of cure of the photopolymer.

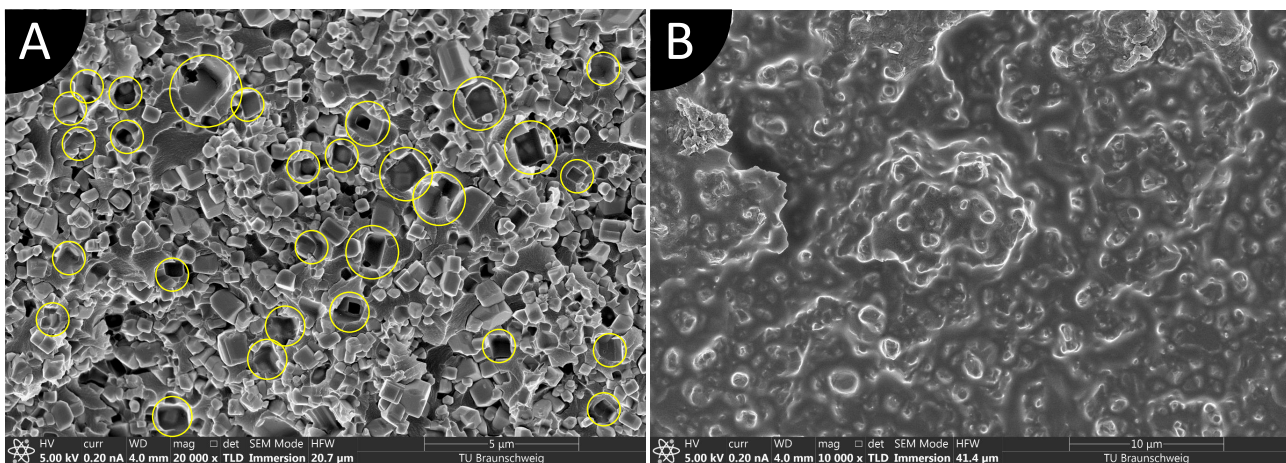


**Figure 2.** Microstructure of: (A) 30KNN6 ( $\times 20,000$ ), (B) 30BTO13 ( $\times 10,000$ ). Yellow circles show clearly visible missing particles.

Some BTO composites show an interesting phenomenon, where the lower side of the composite (opposite side than the UV light is applied) achieves a higher solidification degree, similar to KNN composites (e.g., Figure 2A), while the top part of the composite shows a lower degree of cure (similar to Figure 2B). However, the UV light was exposed from above only. The result is opposite to expected because the highest degree of cure in the composite should happen at the highest UV light exposure—the top area. Therefore, it seems that the UV light, reflected from the table, on which the setup was placed, is stronger than the UV light coming from the source, which does not seem feasible. None of the KNN composites show such behavior and it happened with both BTO particle sizes. The reason is unknown at the moment, but it might be somehow attributed to the higher refractive index of BTO ceramics (Table S1).

All composites with 0.4 wt.% nanofiller loading show a thin layer of unsolidified/gel-like photopolymer in the middle of the composites (see Supplementary Materials), which has a detrimental effect on composite quality and performance. Some composites after manufacturing even split into two thin layers. Therefore, only composites with 0.2 wt.% nanofiller loading are discussed further.

The composites with GNPs achieved relatively high curing depths because the GNPs show huge agglomerates, up to 15  $\mu\text{m}$  in diameter (Figure S15D). Due to poor dispersion, the surface area of UV light absorbing material (GNPs) is overall small and leads to high curing depths, as visible in Figure 1B,G.

Looking at the composites with MWCNTs (Figures S17 and S19), a thin layer of lower curing degree photopolymer in the middle is visible. The results agree with the curing depth data (Figure 1C,H), where composites with MWCNTs show almost the lowest curing depths. Better dispersion of MWCNTs can be observed in BTO composites, which explains the extremely low curing depths visible in Figure 1H, but still some small agglomerates exist.

Both GO materials show better dispersion in KNN composites (see Supplementary Materials), but they are easier recognizable in stiffer KNN composites. BTO composites with GO (Figures S23 and S27) show a very low number of GO particles visible in contrast to KNN composites. It could be speculated that GO2 are somehow agglomerated (layers of GO are not separated properly), which could cause a smaller number of GO2 visible in the cross-section. However, the visibility of GO2 could be poor simply because they are not easily recognizable, especially where the softer matrix is visible. Taking into account very similar curing depths of GO materials, independent of the ceramic particles used (Figure 1D,E,I,J), a conclusion can be drawn that quite homogeneous GO distribution in all composites exists, and it is simply more difficult to distinguish in BTO composites because of the softer polymer matrix.

The worst dispersion is of GNPs, followed by MWCNTs, which show both single rods and agglomerates. Both GO2 and GO3 show much better particle distribution, but the single layers seem to be not properly separated. Therefore, only certain compositions with 0.2 wt.% of nanofillers can be considered for further investigation.

### 3.3. Dielectric Properties

The influence on the dielectric properties of the composites by the addition of carbon-based nanofillers was investigated by measuring relative permittivities  $\epsilon_r$  and dielectric losses  $\tan\delta$ . At this step, the dielectric properties of the composites were measured without applied electrodes (see Section 2.3), therefore, the results are comparable only between the composites manufactured in this study. Because of the measuring method used, the values are around 3–4 times lower than they are with the applied electrodes. Nevertheless, important findings can be obtained from the comparison of the different composites.

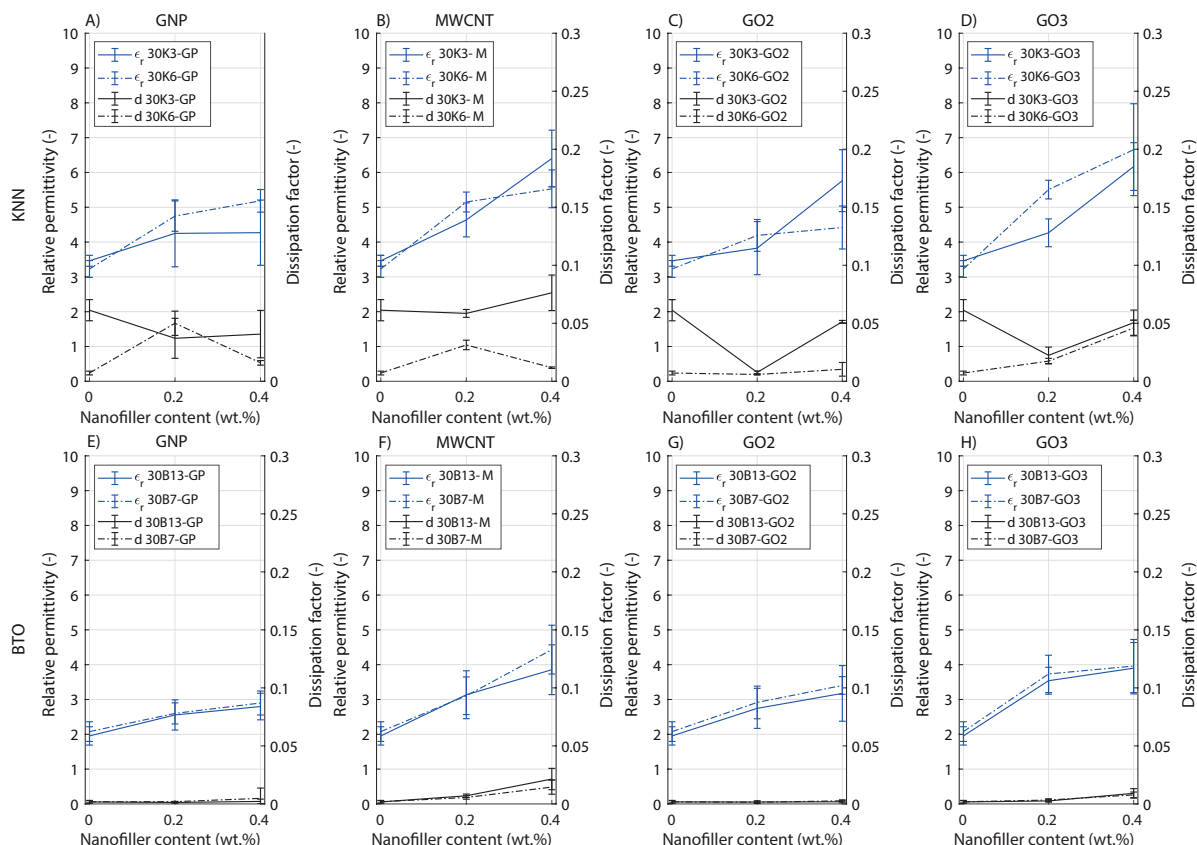


**Figure 3.** Room temperature relative permittivities  $\epsilon_r$  and dielectric losses (dissipation factors  $\tan\delta$ ) of all piezoelectric composites made in this study at 1 kHz. The data are not comparable with the literature since no electrodes were applied to the composites. Measurement points are joined with linear lines for visual purposes only and do not present a linear trend.

Dielectric measurements in Figure 3 show that KNN composites possess higher relative permittivities and dielectric losses than BTO composites. It is quite interesting, because BTO itself, taking the values from the literature (Table S1), has a much higher relative permittivity than KNN. A similar result of higher relative permittivity of KNN composites was found in our previous experiments [76], but BTO particles used in the previous study had different particle sizes and were from a different manufacturer.

One explanation for such results could be a different curing degree of the photopolymer matrix between KNN and BTO composites, as visible in SEM images. Mechanical and dielectric properties of the photopolymer matrix change with a degree of cure. First, as the photopolymer solidifies from a liquid to a gel-like material, both mechanical and dielectric properties increase, up to a certain curing degree, where dielectric properties start to decrease [57]. Most BTO composites show much smoother cross-sections after breaking than KNN composites, indicating lower photopolymer mechanical properties, thus a lower degree of photopolymer cure which could have lower dielectric properties.

This work showed that none of the composites achieved the percolation threshold since there is no abrupt increase in relative permittivity as widely reported in the literature [2,19,41,110–113]. Since some agglomerates of nanofillers are visible, nanofiller-dense zones with percolating behavior may exist (especially MWCNTs).

With simultaneously higher relative permittivities, KNN composites show higher dielectric losses compared to BTO composites. Interestingly, the addition of 0.2 wt.% of any nanofillers to KNN3 composites decreases dielectric losses while increasing relative permittivities, which is highly desirable. The low dielectric losses ensure low current consumption during composite poling and less signal loss during such sensor use. At 0.4 wt.% nanofiller loading in KNN3 composites, dielectric losses start to increase. On the other hand, composites with KNN6 ceramic show mixed results regarding dielectric losses, whereas with both GO nanofillers dielectric losses increased with increasing nanofillers content. An increase in dielectric losses at 0.2 wt.% loading of GNPs or MWCNTs in the KNN6 composite and then a sudden decrease at 0.4 wt.% nanofiller loadings might be attributed to dispersion quality, where composites with 0.2 wt.% nanofiller loading show better dispersion. However, since the values were measured without electrodes applied to the composites, possible measurement errors cannot be discarded due to the low resolution of the measuring devices used in such a configuration. All BTO composites show both relative permittivities and dielectric losses increasing with increasing nanofiller content.

Most of the literature reports an increase in both relative permittivities and dielectric losses with the addition of conductive carbon-based nanofillers [2,19,33,110,114]. However, no literature using KNN and conductive carbon-based nanofillers was found. A small decrease in dielectric losses when using 30 vol.% PZT and 0.02 wt.% MWCNTs (ten times less than in this study) is reported in the literature [115], followed by increasing dielectric losses at higher MWCNTs content; however, the result was not discussed in detail.

Concluding, the addition of conductive nanofillers increases the relative permittivities of the composites, independent of the nanofiller type investigated here. The values of relative permittivities themselves vary slightly, with MWCNTs and GO3 producing the highest relative permittivities at 0.4 wt.% loadings. Dielectric losses mostly increase with the increase in relative permittivities, except for composites filled with KNN3 ceramic, where a decrease in dielectric losses is observed at 0.2 wt.% loadings. Furthermore, KNN6 composites filled with GNPs and MWCNTs show the opposite behavior to KNN3, which could be the result of extremely poor dispersion of GNPs and MWCNTs at 0.4 wt.% GNPs and MWCNTs loadings in KNN6 composites. An increase in the relative permittivities of the composites results from the increased relative permittivity of the photopolymer matrix as the ceramic content was kept constant. The improvement of the permittivity (conductivity) of the matrix is desirable for piezoelectric composite poling [15] and was one of the aims of the addition of the conductive nanofillers.

## 4. Results and Discussion: Detailed Characterization of Selected Composites

### 4.1. Material Selection

For further investigation of the piezoelectric composite performance, the six most promising material combinations were selected, based on the curing depth and relative permittivities. First of all, it was decided to use only two types of ceramics, KNN6 and BTO13, which have the biggest ceramic particles, due to the problems with extremely low curing depths when using smaller particles. Composites with bigger ceramic particles almost always yielded higher curing depths than the same type of ceramics with smaller ceramic particles (Figure 1).

Furthermore, it was decided to investigate two types of conductive nanofillers. Composites filled with GNPs were discarded from further evaluation due to extremely poor dispersion. Therefore, it was decided to use MWCNTs and GO<sub>3</sub>, owing to their lowest cure depth, which most likely indicated the most homogeneous nanofiller dispersion and the highest relative permittivities. The last limitation was to manufacture the composites with a maximum of 0.2 wt.% of nanofiller loading since composites filled with 0.4 wt.% showed uncured photopolymer matrix in the middle of specimens (see Supplementary Materials).

The main difference in this manufacturing process is that UV light exposure time was kept constant as previously (80 s in total), however, the sensors were exposed for 40 s from each side to ensure more homogeneous properties of the specimens.

After the selection of six material compositions, piezoelectric composite sensors were manufactured and covered with silver ink electrodes (see Section 2.2). Their dielectric properties with the applied electrodes were measured and the specimens were poled in a high electric field. Afterward, their piezoelectric properties were measured. Slightly bigger (30 × 20 mm) specimens made out of the same materials, without electrodes, were used to measure Young's modulus.

### 4.2. Dielectric Properties with Applied Electrodes

Dielectric properties of six selected piezoelectric composites with the applied silver ink electrodes are shown in Figure 4. Comparing the results with relative permittivities without electrodes (Figure 3), the different trends of the results are achieved, most likely because of more homogeneous UV light application. First of all, BTO13 composites with nanofillers show slightly higher relative permittivities than KNN6 composites with nanofillers, as expected, since the BTO material itself has a much higher relative permittivity than KNN (Table S1). However, the BTO13 composite without nanofillers shows very similar relative permittivity to the KNN6 composite, while BTO particles themselves have higher relative permittivity than KNN particles. This result most likely is caused by a lower degree of polymer cure in BTO composites.

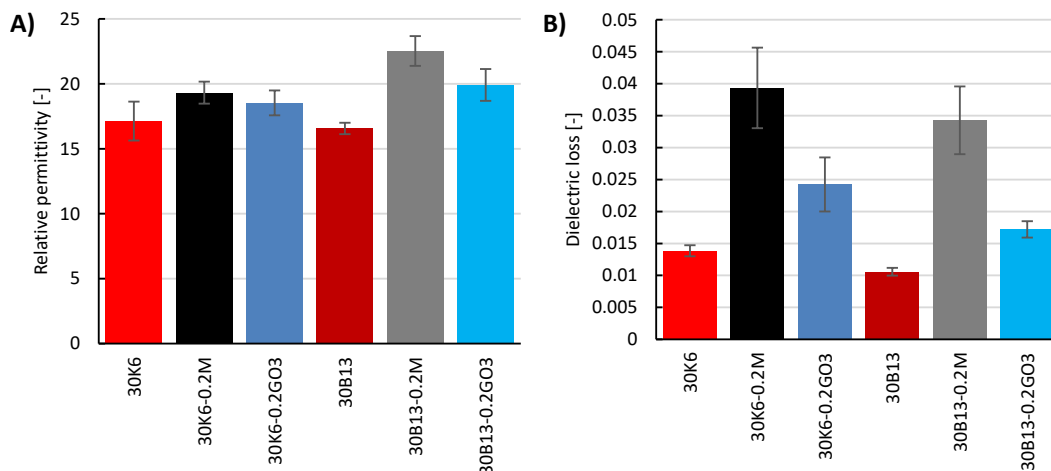


**Figure 4.** Room temperature dielectric properties of piezoelectric composites, with applied silver ink electrodes, before poling at 1 kHz: (A) relative permittivities; (B) dielectric losses.

The relative permittivities of MWCNTs-filled composites are slightly higher than GO3-filled composites, whereas, in previous results without electrodes, it was the opposite. This again could be explained by more homogeneous photopolymer matrix curing, where in the composites without electrodes, MWCNTs absorbed so much UV light, that the parts of the composites were at a lower curing degree with lower relative permittivities. It seems that exposing the composite to the UV light from both sides improves the homogeneity of the photopolymer matrix.

The dielectric losses (see Figure 4B) of all composites are comparably low, which are highly desirable for piezoelectric composite sensors [34]. Dielectric losses follow the trend of increased relative permittivities, where the highest relative permittivities in MWCNTs-filled composites also show the highest dielectric losses, followed by the same trend with GO3-filled composites. KNN6 composites show overall slightly higher dielectric losses than BTO13 composites. However, the difference in dielectric losses between composites filled with different ceramics is not as high as in previous results (see Figure 3). The increase in dielectric losses comes most likely from charge accumulation at the interface of the nanofillers and the matrix (Maxwell–Wagner effect) [34].

The results of dielectric properties prove that both GO3 and MWCNT nanofillers increase the relative permittivities and dielectric losses, the latter showing the highest values. The increase in composite dielectric properties comes from increased relative permittivity of the photopolymer by the addition of nanofillers. According to the literature, high relative permittivities of the matrix help increase poling efficiency and should lead to higher piezoelectric properties [34].

#### 4.3. Young's Modulus

The Young's modulus (elastic modulus) of the composites was measured to determine the piezoelectric charge coefficient  $d_{31}$ . Figure 5 shows Young's modulus of the piezoelectric composites made with BTO13 and KNN6 ceramics, respectively, over the composite thickness. The points represent Young's modulus determined from the measurements. Linear regression was applied to estimate the trend and its change with the addition of conductive nanofillers to the composites. While Young's modulus is a material property that should not vary over the material thickness, the photopolymer resin used in this study as a matrix achieves a varying degree of polymerization over the thickness of the composite, causing Young's modulus to vary with sensor thickness.

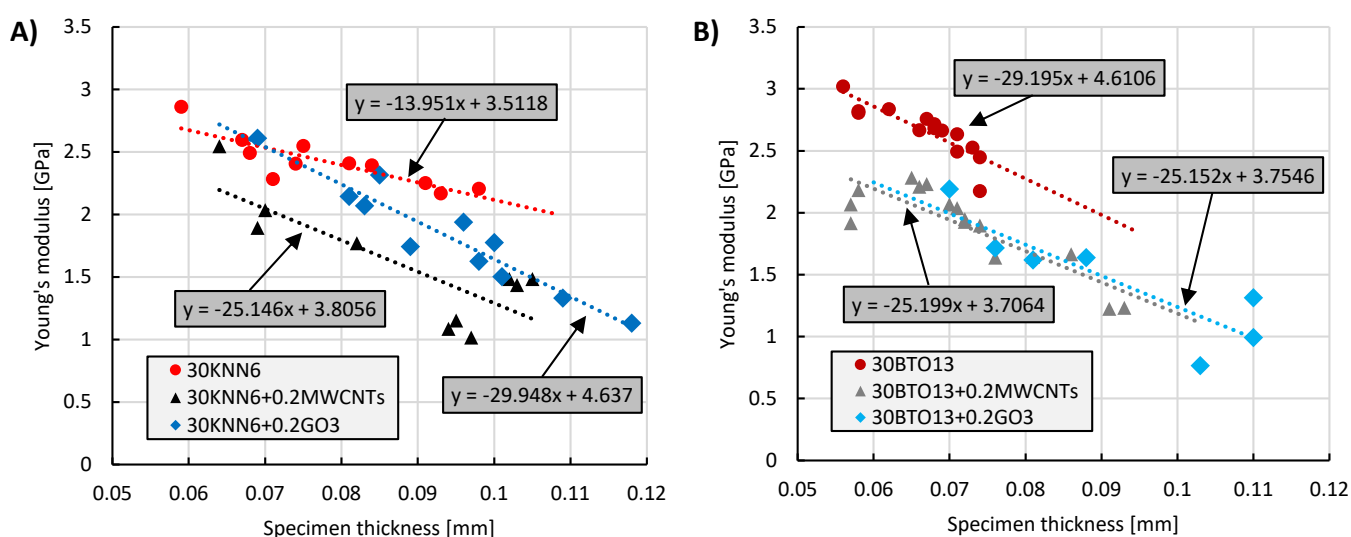


**Figure 5.** Young's modulus of solidified piezoelectric composites filled with: (A) KNN6 ceramic; (B) BTO13 ceramic.

Young's modulus of thinner samples has higher values. The reason is the higher curing degree of the photopolymer in thinner specimens, i.e., more homogeneous solidification over the thickness since all specimens were solidified for 80 s independent of their thickness. Polymerization reaction occurs at varying degrees for the composites studied here: the highest polymerization degree is located at the surfaces and the lowest in the middle.

Composites without conductive nanofillers show the highest Young's modulus values because of the highest polymerization degrees, correlating to the high curing depths of these composites (see Figure 1A,F). With the addition of nanofillers, curing depths decrease, and the photopolymer achieves a lower degree of cure over the cross-section and therefore, lower mechanical properties.

The trend lines added to the graphs provide a lot of information. It is important to mention that the trend of Young's modulus over the thickness can be described linearly only in a small thickness range. From the results not presented here, the trend of Young's modulus follows an inverse polynomial function (decreases over specimen thickness with an increasing rate), with a maximum Young's modulus reaching a plateau at a specific thickness (composite thickness < 20  $\mu\text{m}$ ).

Composites with KNN6 ceramic (Figure 5A) show a varying trend, which is flatter for composites without nanofillers, and steeper for composites with nanofillers. The flatter trend of the KNN6 composite indicates a higher curing degree over its cross-section of this type of composite. Indeed, looking at the curing depth measurements (Figure 1A,F), the KNN6 composite shows a higher curing depth than the BTO13 composite. All graphs of composites with BTO13 (Figure 5B), both without and with nanofillers, show almost the same gradient. However, the trend line of BTO13 without nanofillers should be flatter, and the error could come from the use of thinner specimens since no specimens with a thickness bigger than 0.08 mm were available for testing.

30KNN6-0.2GO3 shows the highest Young's modulus from the composites filled with nanofillers, followed by all other composites, yielding very similar values and trends. However, the curing depths of all four composites with nanofillers are also very similar; therefore, no exact reason for lower properties of 30KNN6-0.2M can be found. One of the reasons could be the reinforcement of the composite by the addition of GO, which only affects KNN6 ceramic particles, but it cannot be justified from these results.

#### 4.4. Sensor Poling and Piezoelectric Properties

As described in Chapter 2, all specimens were poled in a 30 kV/mm electric field for a total of 21 min (4-minute ramp time, 16-minute hold time, 1-minute ramp-down time), based on our previous experiments without nanofillers. Unfortunately, around 95% of all manufactured sensors had at least a small breakdown during poling, indicating too high of an electric field used, which might be a result of not perfect nanofillers dispersion and the existence of some nanofiller-rich zones. However, to compare the results between composites, sensor manufacturing, and poling parameters were kept constant.

Nonetheless, the sensors after small breakdowns are functional, during which a small area of the electrode burns from both sides, and only the area of 1–2  $\text{mm}^2$  of the sensor is not active because of no electrode at that area. This non-active sensor area is subtracted from piezoelectric performance calculations. Taking this into account, the piezoelectric properties of the composites reported in this study might be up to two times lower, when using lower electric fields during poling, which would not cause a dielectric breakdown.

Table 1 summarizes the results of poling. Some piezoelectric composites without nanofillers had some small breakdowns at the maximum electric field, which resulted in shortened polarization time for respective specimens, sometimes to as low as 1-minute hold (instead of 16 min) at 30 kV/mm. However, almost all reached an electric field of 30 kV/mm. On the other hand, all composites with nanofillers experienced a breakdown at voltage ramp-up and only a few sensors with nanofillers reached the electric field of 30 kV/mm, while some (BTO13-0.2MWCNTs and BTO13-0.2GO3) did not reach it at all (Table 1).

**Table 1.** Results of composite poling.

Property	0 wt.% Nanofiller	KNN6 0.2 wt.% MWCNTs	0.2 wt.% GO3	0 wt.% Nanofiller	BTO13 0.2 wt.% MWCNTs	0.2 wt.% GO3
No. of specimens poled full cycle <sup>1</sup>	1/17	1/14	2/28	5/20	0/20	0/20
Max. electric field reached <sup>2</sup> , kV/mm	30	30	30	30	25.6	16.5
Max. current consumed <sup>3</sup> , $\mu$ A	0	0.024	0.23	0	1.816	0.112
Most often breakdown condition	While holding at max electric field	Electric field ramp-up	Electric field ramp-up	While holding at max electric field	Electric field ramp-up	Electric field ramp-up

<sup>1</sup> Number of specimens, that were poled for in total 21 min without any breakdown; <sup>2</sup> Of at least one specimen in the group; <sup>3</sup> Maximum current consumed during poling just before a breakdown, of at least one specimen of the group.

During poling, the reduction in the maximum applicable electric field on the piezoelectric composites with conductive nanofillers was observed, similarly as reported in the literature [34]. None of the composites with BTO13 ceramic and nanofillers reached the maximum electric field of 30 kV/mm, whereas composites made with 0.2 wt.% GO3 reached a maximum of only 16.5 kV/mm before breakdown. The main reason for this is the continuous electric flux paths created by the conductive nanofillers where the poling process becomes more efficient at lower electric fields [34]. It was observed during poling that all composites with nanofillers consume increasingly higher electric current (exponential increase) with increasing electric field, because of the increased dielectric losses  $\tan\delta$ , which might be the main reason for breakdowns before the maximum electric field is reached [15,34]. Holding the electric field constant, current consumption slowly decreases. No experiments were performed to test the influence of the slower ramp-up of the electric field on the current consumption during poling, which might be interesting for future studies. However, no correlation between the poling results and relative permittivity or dielectric loss is found.

From every material composition, 4 to 8 sensors that reached the highest electric fields during poling were selected for piezoelectric measurements. Young's modulus, required for  $d_{31}$  and  $g_{31}$  determination, was calculated for every specimen individually, depending on the specimen thickness, using a linear trend applied to the measurement data (Figure 5A,B).

While most studies with piezoelectric composite materials report piezoelectric charge coefficient  $d_{33}$ , measured with Berlincourt or similar methods, as the main piezoelectric performance parameter, this study reports piezoelectric charge coefficient  $d_{31}$ , measured with a 4-point bending setup, when piezoelectric composites are glued on the surface of the thin glass-fiber beam. Piezoelectric voltage coefficient  $g_{31}$  is more suitable to define the piezoelectric performance of piezoelectric composites since most such composites are used for in-plane sensing applications (e.g., Structural Health Monitoring). Furthermore, because of Young's modulus dependence on the specimen thickness, and the need of it for  $d_{31}$  and  $g_{31}$  determination, the measured sensitivity of the sensors is also added, which directly describes generated charge of the sensor per unit of strain. Both  $d_{31}$  and  $g_{31}$  reported in this study are so-called *effective* constants because the sensors were measured while glued on the substrate. The literature suggests that in such a setup, measured piezoelectric values are approx. 40% lower than by using measuring methods using free-clamped samples [106].

Figure 6 shows piezoelectric charge coefficient  $d_{31}$  (Figure 6A), piezoelectric voltage coefficient  $g_{31}$  (Figure 6B) and sensitivity (Figure 6C). Both  $d_{31}$  and  $g_{31}$  are negative values and are shown positive for visualization purposes only. Table 2 summarizes all results.

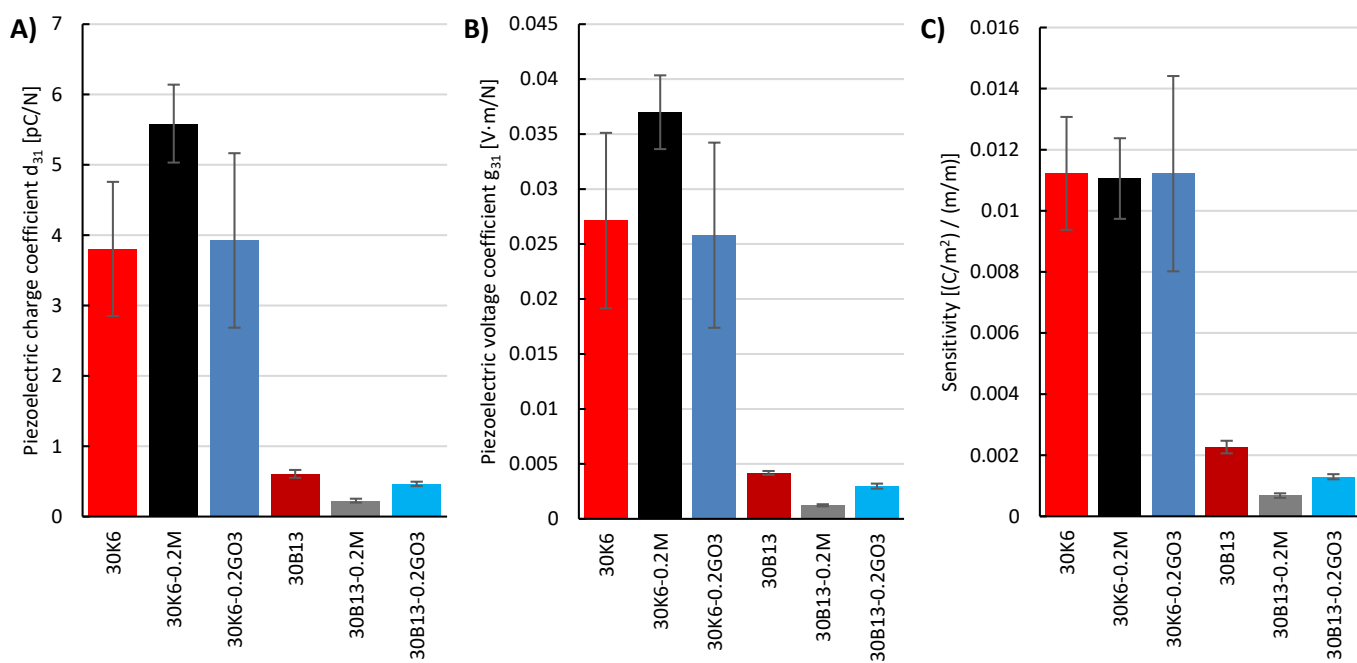


**Figure 6.** Performance of solidified piezoelectric composite materials: (A) piezoelectric charge coefficient  $d_{31}$  (reversed from negative for visualization); (B) piezoelectric voltage coefficient  $g_{31}$  (reversed from negative for visualization); (C) sensitivity.

**Table 2.** Average room temperature properties of solidified piezoelectric composite materials in this study.

Property (Average)	0 wt.%	KNN6	0.2 wt.%	0.2 wt.%	BTO13	
	Nanofiller	MWCNTs	GO3	Nanofiller	MWCNTs	GO3
Thickness, $\mu\text{m}$	101	96	87	68	64	72
Young's modulus, GPa	2.103	1.404	2.046	2.616	2.105	1.952
Relative permittivity <sup>1</sup>	17.132	19.321	18.533	16.563	22.529	19.9145
Dielectric loss <sup>1</sup>	0.014	0.039	0.024	0.011	0.034	0.017
$d_{31}$ , pC/N	-3.8054	-5.586	-3.925	-0.607	-0.227	-0.465
$g_{31}$ , V/m	-0.027	-0.037	-0.0268	-0.004	-0.001	-0.003
Sensitivity, $(\text{C}/\text{m}^2)/(\text{m}/\text{m})$	0.0112	0.0111	0.0112	0.0023	0.0007	0.0013
Sensitivity/thickness, $(\text{C}/\text{m}^2)/(\text{m}/\text{m})/(\text{mm})$	0.111	0.116	0.130	0.033	0.011	0.018

<sup>1</sup> At room temperature, at 1 kHz.

Looking at the values of piezoelectric charge coefficients (Figure 6A), the addition of 0.2 wt% of MWCNTs to KNN6 composites increases the  $d_{31}$  by approx. 47%, followed by only 3% improvement with the addition of GO3. Moreover, 30KNN6-GO3 shows quite a high standard deviation, therefore improvement of  $d_{31}$  cannot be clearly stated. On the other hand, BTO13 composites show overall extremely small  $d_{31}$  values. Surprisingly, the addition of MWCNTs and GO3 reduced  $d_{31}$  by 62% and 24%, respectively, which was not expected. The data sheets of the KNN manufacturer, where epoxy-based composites were filled with KNN and BTO ceramics without nanofillers are not publicly available, and do not contain exact details, but show extreme similarities to the  $d_{31}$  results achieved in this study.

Piezoelectric voltage coefficients (Figure 6B) follow the results of  $d_{31}$ . On the other hand, composite sensitivities (Figure 6C), which were measured without taking into account Young's modulus, show almost the same results for all KNN6 composites, either with or without nanofillers, indicating no real performance improvement by the addition of nanofillers. Sensitivities of BTO13 composites follow the results of piezoelectric charge and voltage coefficients. Almost equal sensitivities of KNN6 composites, not correlating with

piezoelectric charge and voltage coefficients might suggest inaccurate Young's modulus values for 30KNN6-0.2M composites, which could cause higher piezoelectric charge and voltage coefficients.

Since KNN sensors are slightly thicker, sensitivity divided by the sensor thickness is added (Table 2). It shows a similar trend to the results for all BTO composites, but KNN composites show different results: the highest sensitivity is produced by 30K6-0.2GO3 composite, followed by 30K6-0.2M.

All composites with KNN reached a maximum electric field of 30 kV/mm during poling. On the other hand, BTO13 composites with nanofillers reached only lower maximum electric fields during poling (Table 1). The maximum electric field applied during poling has a direct influence on the remnant polarization of the composites, but it still does not explain such a huge decrease in piezoelectric performance. Interestingly, 30KNN6-0.2M shows the highest  $d_{31}$ , while 30BTO13-0.2M possesses the lowest  $d_{31}$ .

Multiple reasons for such results must be discussed. Firstly, the main difference between composites is the piezoelectric ceramic material used. To understand the influence of piezoelectric ceramic on the performance of the composites better, Table S1 with material data taken from literature were added. BTO ceramic itself has more than twice higher  $d_{33}$  than KNN. Therefore, all composites with BTO were expected to show higher performance than KNN composites. Furthermore, the coercive field of BTO is lower than that of KNN. The literature suggests that an electric field twice as high as the coercive field should be applied for the highest performance [29,116–118], and all composites were poled at the exactly same electric field (30 kV/mm). This could explain the lower performance of BTO13-0.2MWCNTs and BTO13-0.2GO3 compared to BTO13 since all specimens broke down before reaching 30 kV/mm. Still, BTO13-0.2MWCNTs reached higher electric fields during poling than BTO13-0.2GO3 but shows lower performance than BTO13-0.2GO3.

BTO13 composites were roughly 25% thinner, but sensor sensitivity over sensor thickness (Table 1) shows that BTO composites have more than 3 times lower sensitivity. Because BTO13 specimens are slightly thinner, they have a higher degree of polymerization (compared to KNN composites) and show slightly higher Young's modulus, especially BTO13-0.2MWCNTs compared to KNN6-0.2MWCNTs. As reported in the literature, a higher Young's modulus of the composite helps to achieve higher piezoelectric performance, because a more rigid matrix transfers more strain to the ceramic particles [66,79,104]. Therefore, a higher Young's modulus of BTO13-0.2MWCNTs does not explain such results either.

Both relative permittivities and dielectric losses (both measured before poling), shown in Figure 4 follow the same trends, with the highest values for MWCNTs filled composites followed by GO3. The trend of relative permittivities follows the  $d_{31}$  results of KNN6 composites presented in Figure 6A, while the values of BTO13 composites do not follow this trend.

The most likely reason for the higher piezoelectric properties of KNN composites is the low relative permittivity of the KNN ceramic itself. A low relative permittivity polymer matrix surrounding the ceramic, with high relative permittivity, reduces the electric field acting on the ceramic particles, because most of the electric field flows through the polymer [15]. Since KNN has much lower relative permittivity than BTO, the difference between ceramic and polymer relative permittivities is smaller, and therefore higher electric fields were acting on the KNN ceramic particles in the composites compared to BTO particles.

All composites with added nanofillers consumed increasingly higher current during poling, opposite to composites without nanofillers, which consumed almost no current during poling at any time. Interestingly, it was observed for 30KNN6-0.2GO3, that the specimens that reached the maximum poling electric field and showed the highest current consumption at that point, showed the lowest  $d_{31}$  values compared to specimens that showed much lower current consumption at peak electric fields. 30BTO13-0.2M composite showed the highest current consumption during poling (Table 1) and possessed the lowest piezoelectric performance. It seems there might a correlation between current consumption

during poling and piezoelectric performance. While the exact reason why some specimens consumed high levels of current during poling is unknown, it is believed to be caused by local agglomerates of the nanofillers, since the dispersion of them was not homogeneous, possibly causing some percolation areas with higher conductivity.

Table 3 compares the results of sensitivity achieved in this study to other studies where sensitivity was reported. Both studies [119,120] investigated similar thickness composite sensors filled with PZT ceramic, at higher PZT loadings, and achieved approx. 3 times higher sensitivities. In the studies, [105,121] used a very similar measuring method to the one used in this study and the sensors had a very similar thickness to the sensors used in this study. Furthermore, a matrix was also acrylic based, and the loading of PZT particles was roughly around 22 vol%. However, all these studies used no conductive nanofillers and were only two-phase composites. Therefore, comparing the results of this study with the literature, still, lead-free piezoelectric composites achieve lower sensitivities, even with the addition of conductive nanofillers and extremely high electric fields used for poling. On the other hand, lead-free KNN ceramic-filled piezoelectric composites seem to be a good candidate for future research.

**Table 3.** Comparison of sensitivity of piezoelectric composite sensors.

Material Composition	Sensitivity, (C/m <sup>2</sup> )/(m/m)	Source
30 vol% KNN6 + Photopolymer	0.0112 ± 0.00185	This study (30KNN6)
30 vol% KNN6 + 0.2 wt% MWCNTs + Photopolymer	0.0111 ± 0.00132	This study (30KNN6-0.2M)
30 vol% KNN6 + 0.2 wt% GO3 + Photopolymer	0.0112 ± 0.00171	This study (30KNN6-0.2GO3)
52 vol% PZT + Epoxy	0.034	[119]
52 vol% PZT + Epoxy	0.035	[120]
22 vol% PZT + Acrylic paint	0.0183 ± 0.0015	[105]
22 vol% PZT + Acrylic paint	0.0212 ± 0.0008	[121]

## 5. Conclusions

This study investigated the dielectric, mechanical, and piezoelectric properties of lead-free piezoelectric composite sensors. Ceramic particles and conductive carbon-based nanofillers were added to UV light curable photopolymer resin to form piezoelectric sensors. Results show that bigger KNN particles (at 30 vol% loading) and Multi-Walled Carbon nanotubes (MWCNTs) (at 0.2 wt% loading) produce the highest piezoelectric performance ( $d_{31} = -5.59 \text{ pC/N}$ ), while all composites filled with BTO produced values lower than  $-1 \text{ pC/N}$ . However, looking at the sensitivity values, no real improvement is observed with the addition of conductive nanofillers, while GO3 in KNN composites is worth further investigation.

The addition of nanofillers to the composites strongly reduces their curing depth, making homogeneous solidification of thicker composites impossible, and in turn reducing Young's modulus of the composites. Nanofillers help to increase the dielectric properties of the photopolymer matrix, which should make poling at lower voltages more efficient, but no real benefit was observed. None of the investigated nanofillers achieved homogeneous dispersion, as observed by SEM images.

Comparing the sensitivity achieved by KNN composites with the literature, lower performance than two-phase PZT-filled composites was achieved, but KNN-filled composites are very promising for future research as a lead-free substitute for piezoelectric composites. The low relative permittivity of the KNN ceramic might be the key factor, why KNN composites produced higher piezoelectric properties than BTO composites and is worth further investigation.

**Supplementary Materials:** The following supporting information can be downloaded at: <https://www.mdpi.com/article/10.3390/jcs7020089/s1>. Detailed description of Materials and Methods section; Figure S1: SEM images of piezoelectric ceramics used in this study; Table S1. Properties of piezoelectric ceramics; Figure S2. X-ray diffraction pattern at room temperature of ceramics used in this study; Table S2. Properties of nanofillers; Figures S3–S6: SEM images of nanofillers used in this study; Figure S7. Schematics of UV light curable suspension preparation; Figure S8. Process of UV light curable suspension preparation; Figure S9. Schematic representation of piezoelectric composite sensor forming and solidification; Figure S10. Tape-casting of piezoelectric composite sensors; Figure S11. Principle of measurement of dielectric properties without applied electrodes; Figures S12–S28: SEM images of cross-sections of investigated composites; Table S3. Properties of piezoelectric composites with measurement errors. References [122–125] are cited in the Supplementary Materials.

**Author Contributions:** Conceptualization, software, validation, formal analysis, investigation, writing—original draft preparation, visualization, R.M. and L.P.; methodology, resources, supervision, project administration, R.M.; data curation, L.P.; funding acquisition, M.S.; writing—review and editing, R.M., L.P., and M.S. All authors have read and agreed to the published version of the manuscript.

**Funding:** This research was funded by the German Research Foundation (Deutsche Forschungsgemeinschaft, DFG), grant number 389409970.

**Institutional Review Board Statement:** Not applicable.

**Informed Consent Statement:** Not applicable.

**Acknowledgments:** We acknowledge support by the Open Access Publication Funds of Technische Universität Braunschweig. The authors are grateful to Nippon Chemical Industrial Co., Ltd. (Tokyo, Japan) for providing Potassium Sodium Niobate (KNN) piezoelectric ceramic materials used in this research. We thank Marion Görke for the help with XRD measurements, Louise Niemeyer and Bogdan Semenenko for the help with SEM images. We also thank Yangyang Fang and Armin Stein for the help with BTO composite manufacturing and measurements. We thank Weijun Liu for the help with piezoelectric measurements.

**Conflicts of Interest:** The authors declare no conflict of interest. The funders had no role in the design of the study; in the collection, analyses, or interpretation of data; in the writing of the manuscript, or in the decision to publish the results.

## References

1. Sundar, U.; Cook-Chennault, K.A.; Banerjee, S.; Refour, E. Dielectric and piezoelectric properties of percolative three-phase piezoelectric polymer composites. *J. Vac. Sci. Technol. B* **2016**, *34*, 041232. [[CrossRef](#)]
2. Tang, J.; Liu, J.; Huang, H. Dielectric, Piezoelectric and Ferroelectric Properties of Flexible 0–3 Type PZT/PVDF Composites Doped with Graphene. *J. Electron. Mater.* **2019**, *48*, 4033–4039. [[CrossRef](#)]
3. Tiller, B.; Reid, A.; Zhu, B.; Guerreiro, J.; Domingo-Roca, R.; Curt Jackson, J.; Windmill, J.F.C. Piezoelectric microphone via a digital light processing 3D printing process. *Mater. Des.* **2019**, *165*, 1–7. [[CrossRef](#)]
4. Wang, Z.; Narita, F. Corona Poling Conditions for Barium Titanate/Epoxy Composites and their Unsteady Wind Energy Harvesting Potential. *Adv. Eng. Mater.* **2019**, *21*, 1900169. [[CrossRef](#)]
5. Ponraj, B.; Bhimireddi, R.; Varma, K.B.R. Effect of nano- and micron-sized K<sub>0.5</sub>Na<sub>0.5</sub>NbO<sub>3</sub> fillers on the dielectric and piezoelectric properties of PVDF composites. *J. Adv. Ceram.* **2016**, *5*, 308–320. [[CrossRef](#)]
6. Lin, J.; Chen, G.; Yang, W.; Li, H.; Lei, Q. New potassium sodium niobate/poly(vinylidene fluoride) functional composite films with high dielectric permittivity. *J. Polym. Res.* **2016**, *23*, 152. [[CrossRef](#)]
7. Newnham, R.E.; Safari, A.; Giniewicz, J.; Fox, B.H. Composite piezoelectric sensors. *Ferroelectrics* **1984**, *60*, 15–21. [[CrossRef](#)]
8. Newnham, R.E.; Skinner, D.P.; Cross, L.E. Connectivity and piezoelectric-pyroelectric composites. *Mater. Res. Bull.* **1978**, *13*, 525–536. [[CrossRef](#)]
9. James, N.K. Piezoelectric and Dielectric Properties of Polymer-Ceramic Composites for Sensors. Master's Thesis, Delft University of Technology, Delft, The Netherlands, 17 June 2015.
10. Karapuzha, A.S. Exploration of Non-MPB PZT Compositions for High Piezoelectric Voltage Sensitive 0-3 Composites. Master's Thesis, Delft University of Technology, Delft, The Netherlands, 17 December 2014.
11. Mascarenhas, N.T. Highly Flexible Lead-Free Piezoelectric Composites: For Vibration Damping and Noise Cancellation Applications. Master's Thesis, Delft University of Technology, Delft, The Netherlands, 27 November 2015.
12. Lammering, R.; Gabbert, U.; Sinapius, M.; Schuster, T.; Wieach, P. *Lamb-Wave Based Structural Health Monitoring in Polymer Composites*; Springer: Berlin/Heidelberg, Germany, 2018.

13. Banerjee, S. An Experimental and Theoretical Analysis of Two and Three Phase Epoxy Based Piezoelectric Composites. Master's Thesis, The State University of New Jersey, New Brunswick, NJ, USA, May 2013. [\[CrossRef\]](#)
14. Han, K.; Safari, A.; Rimann, R.E. Colloidal Processing for Improved Piezoelectric Properties of Flexible 0-3 Ceramic-Polymer Composites. *J. Am. Ceram. Soc.* **1991**, *74*, 1699–1702. [\[CrossRef\]](#)
15. Sa-Gong, G.; Safari, A.; Jang, S.J.; Newnham, R.E. Poling flexible piezoelectric composites. *Ferroelectr. Lett. Sect.* **1986**, *5*, 131–142. [\[CrossRef\]](#)
16. Takahashi H. Development of lead-free BaTiO<sub>3</sub> ceramics possessing enhanced piezoelectric properties. *Electron. Comm. Jpn.* **2012**, *95*, 20–26. [\[CrossRef\]](#)
17. Aksel, E.; Jones, J.L. Advances in lead-free piezoelectric materials for sensors and actuators. *Sensors* **2010**, *10*, 1935–1954. [\[CrossRef\]](#) [\[PubMed\]](#)
18. Maeder, M.D.; Damjanovic, D.; Setter, N. Lead Free Piezoelectric Materials. *J. Electroceram.* **2004**, *13*, 385–392. [\[CrossRef\]](#)
19. Liu, J.; Tian, G.; Qi, S.; Wu, Z.; Wu, D. Enhanced dielectric permittivity of a flexible three-phase polyimide-graphene-BaTiO<sub>3</sub> composite material. *Mater. Lett.* **2014**, *124*, 117–119. [\[CrossRef\]](#)
20. Luo, C.; Hu, S.; Xia, M.; Li, P.; Hu, J.; Li, G.; Jiang, H.; Zhang, W. A Flexible Lead-Free BaTiO<sub>3</sub>/PDMS/C Composite Nanogenerator as a Piezoelectric Energy Harvester. *Energy Technol.* **2018**, *6*, 922–927. [\[CrossRef\]](#)
21. Ferreira, O.B.; Venkat, R.S.; Boller C. Development of the Fabrication Process and Characterization of Piezoelectric BaTiO<sub>3</sub>/Epoxy Composite Used for Coated Ultrasonic Transducer Patterns in Structural Health Monitoring. In Proceedings of 19th World Conference on Non-Destructive Testing, Munich, Germany, 13–17 June 2016. [\[CrossRef\]](#)
22. Wang, Z.; Abe, S.; Narita, F. On the Energy Harvesting Potential of Lead-Free Piezoelectric Composites from Air-Flow and Temperature Change. *Res. Dev. Mater. Sci.* **2018**, *5*, 000607. [\[CrossRef\]](#)
23. Deutz, D.B.; Mascarenhas, N.T.; van der Zwaag, S.; Groen, W.A. Enhancing energy harvesting potential of (K,Na,Li)NbO<sub>3</sub>-epoxy composites via Li substitution. *J. Am. Ceram. Soc.* **2017**, *100*, 1108–1117. [\[CrossRef\]](#)
24. Gupta, M.K.; Kim, S.W.; Kumar, B. Flexible High-Performance Lead-Free Na<sub>0.47</sub>K<sub>0.47</sub>Li<sub>0.06</sub>NbO<sub>3</sub> Microcube-Structure-Based Piezoelectric Energy Harvester. *ACS Appl. Mater. Interfaces* **2016**, *8*, 1766–1773. [\[CrossRef\]](#)
25. Jeong, C.K.; Park, K.I.; Ryu, J.; Hwang, G.T.; Lee, K.J. Large-Area and Flexible Lead-Free Nanocomposite Generator Using Alkaline Niobate Particles and Metal Nanorod Filler. *Adv. Funct. Mater.* **2014**, *24*, 2620–2629. [\[CrossRef\]](#)
26. Bhalla, S.; Moharana, S.; Talakokula, V.; Kaur, N. *Piezoelectric Materials: Applications in SHM, Energy Harvesting and Bio-mechanics*, 1st ed.; Athena Academic Ltd. and John Wiley & Sons Ltd.: Hoboken, NJ, USA, 2017; pp. 225–233. [\[CrossRef\]](#)
27. Egerton, L.; Dillon, D.M. Piezoelectric and Dielectric Properties of Ceramics in the System Potassium-Sodium Niobate. *J. Am. Ceram. Soc.* **1959**, *42*, 438–442. [\[CrossRef\]](#)
28. Bechmann, R. Elastic, Piezoelectric, and Dielectric Constants of Polarized Barium Titanate Ceramics and Some Applications of the Piezoelectric Equations. *J. Acoust. Soc. Am.* **1956**, *28*, 347–350. [\[CrossRef\]](#)
29. Jaffe, H. Piezoelectric Ceramics. *J. Am. Ceram. Soc.* **1958**, *41*, 494–498. [\[CrossRef\]](#)
30. Qin, Y.; Zhang, J.; Yao, W.; Wang, C.; Zhang, S. Domain Structure of Potassium-Sodium Niobate Ceramics Before and After Poling. *J. Am. Ceram. Soc.* **2015**, *98*, 1027–1033. [\[CrossRef\]](#)
31. Nan, C.-W. Shen, Y.; Ma, J. Physical Properties of Composites Near Percolation. *Annu. Rev. Mater. Sci.* **2010**, *40*, 131–151. [\[CrossRef\]](#)
32. Dang, Z.-M.; Shen, Y.; Nan, C.-W. Dielectric behavior of three-phase percolative Ni–BaTiO<sub>3</sub>/polyvinylidene fluoride composites. *Appl. Phys. Lett.* **2002**, *81*, 4814–4816. [\[CrossRef\]](#)
33. Petrossian, G.; Aliheidari, N.; Ameli, A. Thermoplastic Polyurethane/Lead Zirconate Titanate/Carbon Nanotube Composites with Very High Dielectric Permittivity and Low Dielectric Loss. *J. Compos. Sci.* **2020**, *4*, 137. [\[CrossRef\]](#)
34. Sakamoto, W.K.; de Souza, E.; Das-Gupta, D.K. Electroactive properties of flexible piezoelectric composites. *Mater. Res.* **2001**, *4*, 201–204. [\[CrossRef\]](#)
35. Sakamoto, W.K.; Marin-Franch, P.; Das-Gupta, D.K. Characterization and application of PZT/PU and graphite doped PZT/PU composite. *Sens. Actuators Phys.* **2002**, *100*, 165–174. [\[CrossRef\]](#)
36. De Melo, C.C.N.; Beatrice, C.A.G.; Pessan, L.A.; de Oliveira, A.D.; Machado F.M. Analysis of Nonisothermal Crystallization Kinetics of Graphene Oxide-Reinforced Polyamide 6 Nanocomposites. *Thermochim. Acta* **2018**, *667*, 111–121. [\[CrossRef\]](#)
37. Gómez, H.; Ram, M.K.; Alvi, F.; Villalba, P.; Stefanakos, E.; Kumar, A. Graphene-conducting polymer nanocomposite as novel electrode for supercapacitors. *J. Power Source* **2011**, *196*, 4102–4108. [\[CrossRef\]](#)
38. Patsidis, A.C.; Kalaitzidou, K.; Anastassopoulos, D.L.; Vradis, A.A.; Psarras, G.C. Graphite nanoplatelets and/or barium titanate/polymer nanocomposites: fabrication, thermomechanical properties, dielectric response and energy storage. *J. Chin. Adv. Mater. Soc.* **2014**, *2*, 207–221. [\[CrossRef\]](#)
39. Ravindran, A.R.; Feng, C.; Huang, S.; Wang, Y.; Zhao, Z.; Yang, J. Effects of Graphene Nanoplatelet Size and Surface Area on the AC Electrical Conductivity and Dielectric Constant of Epoxy Nanocomposites. *Polymers* **2018**, *10*, 477. [\[CrossRef\]](#) [\[PubMed\]](#)
40. Babu, I. Piezoelectric Composites: Design, Fabrication and Performance Analysis. Ph.D. Thesis, Eindhoven University of Technology, Eindhoven, The Netherlands, 1 January 2013. [\[CrossRef\]](#)

41. Xu, W.; Ding, Y.; Jiang, S.; Chen, L.; Liao, X.; Hou, H. Polyimide/BaTiO<sub>3</sub>/MWCNTs three-phase nanocomposites fabricated by electrospinning with enhanced dielectric properties. *Mater. Lett.* **2014**, *135*, 158–161. [CrossRef]
42. Liu, J.; Wu, Y.; Shen, J.; Gao, Y.; Zhang, L.; Cao, D. Polymer-nanoparticle interfacial behavior revisited: A molecular dynamics study. *Phys. Chem. Chem. Phys.* **2011**, *13*, 13058–13069. [CrossRef] [PubMed]
43. De Oliveira, A.D.; Beatrice, C.A.G. Polymer Nanocomposites with Different Types of Nanofiller. In *Nanocomposites—Recent Evolutions*; Sivasankaran, S., Ed.; IntechOpen: London, UK, 2019; pp. 103–128.
44. Banerjee, S.; Cook-Chennaul, K.A. Influence of Al Particle Size and Lead Zirconate Titanate (PZT) Volume Fraction on the Dielectric Properties of PZT-Epoxy-Aluminum Composites. *J. Eng. Mater. Technol.* **2011**, *133*, 041016. [CrossRef]
45. Cui, X.; Zhang, C.; Hao, R.; Hou, Y. Liquid-phase exfoliation, functionalization and applications of graphene. *Nanoscale* **2011**, *3*, 2118. [CrossRef] [PubMed]
46. Chiappone, A.; Roppolo, I.; Naretto, E.; Fantino, E.; Calignano, F.; Sangermano, M.; Pirri, F. Study of graphene oxide-based 3D printable composites: Effect of the in situ reduction. *Compos. Part B* **2017**, *124*, 9–15. [CrossRef]
47. Li, H.; Bubeck, C. Photoreduction Process of Graphene Oxide and Related Applications. *Macromol. Res.* **2013**, *21*, 290–297. [CrossRef]
48. Eng, H.; Maleksaeedi, S.; Yu, S.; Choong, Y.Y.C.; Wiria, F.E.; Kheng, R.E.; Wei, J.; Su, P.-C.; Tham, P.H. Development of CNTs-filled photopolymer for projection stereolithography. *Rapid Prototyp. J.* **2017**, *23*, 129–136. [CrossRef]
49. Lin, D.; Jin, S.; Zhang, F.; Wang, C.; Wang, Y.; Zhou, C.; Cheng, G.J. 3D stereolithography printing of graphene oxide reinforced complex architectures. *Nanotechnology* **2015**, *26*, 434003. [CrossRef]
50. Manapat, J.Z.; Chen, Q.; Ye, P.; Advincula, R.C. 3D Printing of Polymer Nanocomposites via Stereolithography. *Macromol. Mater. Eng.* **2017**, *302*, 1600553. [CrossRef]
51. Chiulan, I.; Voicu, S.I.; Batalu, D. The Use of Graphene and Its Derivatives for the Development of Polymer Matrix Composites by Stereolithographic 3D Printing. *Appl. Sci.* **2022**, *12*, 3521. [CrossRef]
52. Hyeonseo, J.; Sunghun, C. Comparative Studies on Polyurethane Composites Filled with Polyaniline and Graphene for DLP-Type 3D Printing. *Polymers* **2020**, *12*, 67. [CrossRef]
53. Oliveira, A.D.; Beatrice, C.A.G.; Passador, F.R.; Pessan, L.A. Polyetherimide-based nanocomposites materials for hydrogen storage. In Proceedings of the Regional Conference Graz, Graz, Austria, 21–25 September 2015; Volume 1779, p. 040006. [CrossRef]
54. Min, Y.; Akbulut, M.; Kristiansen, K.; Golan, Y.; Israelachvili, J. The role of interparticle and external forces in nanoparticle assembly. *Nat. Mater.* **2008**, *7*, 527–538. [CrossRef] [PubMed]
55. Feng, Z.; Li, Y.; Xin, C.; Tang, D.; Xiong, W.; Zhang, H. Fabrication of Graphene-Reinforced Nanocomposites with Improved Fracture Toughness in Net Shape for Complex 3D Structures via Digital Light Processing. *J. Carbon Res.* **2019**, *5*, 25. [CrossRef]
56. Huang, Y.Y.; Terentjev, E.M. Dispersion of Carbon Nanotubes: Mixing, Sonication, Stabilization, and Composite Properties. *Polymers* **2012**, *4*, 275–295. [CrossRef]
57. Mitkus, R.; Scharnofske, M.; Sinapius, M. Characterization 0.1 wt.% Nanomaterial/Photopolymer Composites with Poor Nanomaterial Dispersion: Viscosity, Cure Depth and Dielectric Properties. *Polymers* **2021**, *13*, 3948. polym13223948. [CrossRef]
58. Ha, J.-H.; Lee, S.-E.; Park, S.-H. Effect of Dispersion by Three-Roll Milling on Electrical Properties Filler Length of Carbon Nanotube Composites. *Materials* **2019**, *12*, 3823. [CrossRef]
59. Goh, P.S.; Ng, B.C.; Ismail, A.F.; Aziz, M.; Sanip, S.M. Surfactant dispersed multi-walled carbon nanotube/polyetherimide nanocomposite membrane. *Solid State Sci.* **2010**, *12*, 2155–2162. [CrossRef]
60. Suherman, H.; Dweiri, R.; Mahyoedin, Y.; Duskiardi, D. Investigation of electrical-mechanical performance of epoxy-based nanocomposites filled with hybrid electrically conductive fillers. *Mater. Res. Express* **2019**, *6*, 115010. [CrossRef]
61. Kaur, I.; Ellis, L.-J.; Romer, I.; Tantra, R.; Carriere, M.; Allard, S.; Mayne-L’Hermite, M.; Minelli, C.; Unger, W.; Potthoff, A.; et al. Dispersion of Nanomaterials in Aqueous Media: Towards Protocol Optimization. *J. Vis. Exp.* **2017**, *130*, e56074. [CrossRef]
62. Miller-Ihli, N. Automated Ultrasonic Mixing Accessory for Slurry Sampling into a Graphite Furnace Atomic Absorption Spectrometer. *J. Anal. At. Spectrom.* **1989**, *4*, 295–297. [CrossRef]
63. Chen, Z.; Song, X.; Lei, L.; Chen, X.; Fei, C.; Chiu, C.T.; Qian, X.; Ma, T.; Yang, Y.; Shung, K.; et al. 3D Printing of Piezoelectric Element for Energy Focusing and Ultrasonic Sensing. *Nano Energy* **2016**, *27*, 78–86. [CrossRef]
64. Dang, Z.-M.; Yuan, J.-K.; Zha, J.-W.; Zhou, T.; Li, S.-T.; Hu, G.-H. Fundamentals, process and applications of high-permittivity polymer-matrix composites. *Prog. Mater. Sci.* **2012**, *57*, 660–723. [CrossRef]
65. Arlt, K.; Wegener, M. Piezoelectric PZT/PVDF-copolymer 0-3 Composites: Aspects on Film Preparation and Electrical Poling. *IEEE Trans. Dielectr. Electr. Insul.* **2010**, *17*, 1178–1184. [CrossRef]
66. Yao, D.; Cui, H.; Hensleigh, R.; Smith, P.; Alford, S.; Bernero, D.; Bush, S.; Mann, K.; Wu, F.; Chin-Nieh, M.; et al. Achieving the Upper Bound of Piezoelectric Response in Tunable, Wearable 3D Printed Nanocomposites. *Adv. Funct. Mater.* **2019**, *29*, 1903866. [CrossRef]
67. Chen, Z.; Li, Z.; Li, J.; Liu, C.; Lao, C.; Fu, Y.; Liu, C.; Li, Y.; Wang, P.; He, Y. 3D printing of ceramics: A review. *J. Eur. Ceram. Soc.* **2019**, *39*, 661–687. [CrossRef]
68. Cui, H.; Hensleigh, R.; Yao, D.; Maurya, D.; Kumar, P.; Kang, M.G.; Priya, S.; Zheng, X.R. Three-dimensional printing of piezoelectric materials with designed anisotropy and directional response. *Nat. Mater.* **2019**, *18*, 234–241. [CrossRef]

69. Mitkus, R.; Pierou, A.; Feder, J.; Sinapius, M. Investigation and Attempt to 3D Print Piezoelectric 0-3 Composites Made of Photopolymer Resins and PZT. In Proceedings of the Conference on Smart Materials, Adaptive Structures and Intelligent Systems, Irvine, CA, USA, 15 September 2020. [CrossRef]
70. Liska, R.; Schuster, M.; Inführ, R.; Turecek, C.; Fritscher, C.; Seidl, B.; Schmidt, V.; Kuna, L.; Haase, A.; Varga, F.; et al. Photopolymers for rapid prototyping. *J. Coat. Technol. Res.* **2007**, *4*, 505–510. [CrossRef]
71. Hull, C.W. Apparatus for Production of Three-Dimensional Objects by Stereolithography. US Patent US4575330A, 11 March 1986. Available online: <https://patents.google.com/patent/US4575330A/en> (accessed on 26 January 2023).
72. Stansbury, J.W.; Idacavage, M.J. 3D printing with polymers: Challenges among expanding options and opportunities. *Dent. Mater. J.* **2016**, *32*, 54–65. [CrossRef]
73. Song, X.; Chen, Z.; Lei, L.; Shung, K.; Zhou, Q.; Chen, Y. Piezoelectric component fabrication using projection-based stereolithography of barium titanate ceramic suspensions. *Rapid Prototyp. J.* **2017**, *23*, 44–53. [CrossRef]
74. Fantino, E.; Chiappone, A.; Calignano, F.; Fontana, M.; Pirri, F.; Roppolo, I. In Situ Thermal Generation of Silver Nanoparticles in 3D Printed Polymeric Structures. *Materials* **2016**, *9*, 589. [CrossRef] [PubMed]
75. Jang, J.H.; Wang, S.; Pilgrim, S.M.; Schulze, W.A. Preparation and Characterization of Barium Titanate Suspensions for Stereolithography. *J. Am. Ceram. Soc.* **2000**, *83*, 1804–1806. [CrossRef]
76. Mitkus, R.; Sinapius, M. Piezoelectric Ceramic/Photopolymer Composites Curable with UV Light: Viscosity, Curing Depth, and Dielectric Properties. *J. Compos. Sci.* **2022**, *6*, 212. [CrossRef]
77. Yang, Y.; Chen, Z.; Song, X.; Zhu, B.; Hsiao, T.; Wu, P.-I.; Xiong, R.; Shi, J.; Chen, Y.; Zhou, Q.; et al. Three dimensional printing of high dielectric capacitor using projection based stereolithography method. *Nano Energy* **2016**, *22*, 414–421. [CrossRef]
78. Kim, K.; Zhu, W.; Qu, X.; Aaronson, C.; McCall, W.R.; Chen, S.; Sirbuly, D.J. 3D optical printing of piezoelectric nanoparticle-polymer composite materials. *ACS Nano* **2014**, *8*, 9799–9806. [CrossRef] [PubMed]
79. Kim, K.; Middlebrook, J. L.; Chen, J. E.; Zhu, W.; Chen, S.; Sirbuly, D.J. Tunable Surface and Matrix Chemistries in Optically Printed (0-3) Piezoelectric Nanocomposites. *ACS Appl. Mater. Interfaces* **2016**, *8*, 33394–33398. [CrossRef] [PubMed]
80. Mitkus, R.; Taleb A.A.; Sinapius, M. An Attempt to Topology Optimize 3D Printed Piezoelectric Composite Sensors for Highest D31 Output. In Proceedings of the ASME 2021 Conference on Smart Materials, Adaptive Structures and Intelligent Systems. ASME 2021 Conference on Smart Materials, Adaptive Structures and Intelligent Systems, Virtual, Online, 14–15 September 2021. [CrossRef]
81. Fantino, E.; Chiappone, A.; Roppolo, I.; Manfredi, D.; Bongiovanni, R.; Pirri, C.F.; Calignano, F. 3D Printing of Conductive Complex Structures with In Situ Generation of Silver Nanoparticles. *Adv. Mater.* **2016**, *28*, 3712–3717. [CrossRef]
82. Travitzky, N.; Bonet, A.; Dermeik, B.; Fey, T.; Filbert-Demut, I.; Schlier, L.; Schlöldt, T.; Greil, P. Additive Manufacturing of Ceramic-Based Materials. *Adv. Eng. Mater.* **2014**, *16*, 729–754. [CrossRef]
83. Roloff, T.; Mitkus, R.; Lion, J.; Sinapius, M. 3D printable piezoelectric composite sensors for guided ultrasonic wave detection. In Proceedings of the 8th International Electronic Conference on Sensors and Applications, Basel, Switzerland, 1–15 November 2021. [CrossRef]
84. Schmidt, Daniel, Modenselektive Übertragung von Lambwellen in Faserverbundstrukturen. PhD Thesis , Teschnische Universität Braunschweig, Braunschweig, Germany, 2014.
85. Takahashi, H.; Yoshiki, N.; Tani, J.; Matsuta, K.; Qiu, J.; Tsurekawa, S. Lead-Free Barium Titanate Ceramics with Large Piezoelectric Constant Fabricated by Microwave Sintering. *Jpn. J. Appl. Phys.* **2006**, *45*, L30–L32. [CrossRef]
86. Babu, I.; van den Ende, D.A.; de With, G. Processing and characterization of piezoelectric 0-3 PZT/LCT/PA composites. *J. Phys. D Appl. Phys.* **2010**, *43*, 425402. [CrossRef]
87. Halloran, J.W. Ceramic Stereolithography: Additive Manufacturing for Ceramics by Photopolymerization. *Annu. Rev. Mater. Res.* **2016**, *46*, 19–40. [CrossRef]
88. Badev, A.; Aboualiatim, Y.; Chartier, T.; Lecamp, L.; Lebaudy, P.; Chaput, C.; Delage, C. Photopolymerization kinetics of a polyether acrylate in the presence of ceramic fillers used in stereolithography. *J. Photochem. Photobiol. A Chem.* **2011**, *222*, 117–122. [CrossRef]
89. Sun, C.; Zhang, X. Experimental and numerical investigations on microstereolithography of ceramics. *J. Appl. Phys.* **2002**, *92*, 4796. [CrossRef]
90. Griffith, M.L.; Halloran, J.W. Freeform Fabrication of Ceramics via Stereolithography. *J. Am. Ceram. Soc.* **1996**, *79*, 2601–2608. [CrossRef]
91. Gonzalez, G.; Chiappone, A.; Roppolo, I.; Fantino, E.; Bertana, V.; Perrucci, F.; Scaltrito, L.; Pirri, F.; Sangermano, M. Development of 3D printable formulations containing CNT with enhanced electrical properties. *Polymer* **2017**, *109*, 246–253. [CrossRef]
92. Bomlai, P.; Wichianrat, P.; Muensit, S.; Milne, S.J. Effect of Calcination Conditions and Excess Alkali Carbonate on the Phase Formation and Particle Morphology of Na<sub>0.5</sub>K<sub>0.5</sub>NbO<sub>3</sub> Powders. *J. Am. Ceram. Soc.* **2007**, *90*, 1650–1655. [CrossRef]
93. Kumar, P.; Pattanaik, M. Synthesis and characterizations of KNN ferroelectric ceramics near 50/50 MPB. *Ceram. Int.* **2013**, *39*, 65–69. [CrossRef]
94. Skidmore, T.A.; Milne, S.J. Phase development during mixed-oxide processing of a [Na<sub>0.5</sub>K<sub>0.5</sub>NbO<sub>3</sub>]<sub>1-x</sub> – [LiTaO<sub>3</sub>]<sub>x</sub> powder. *J. Mater. Res.* **2007**, *22*, 2265–2272. [CrossRef]
95. Dwivedi, S.; Pareek, T.; Kumar, S. Structure, dielectric, and piezoelectric properties of K<sub>0.5</sub>Na<sub>0.5</sub>NbO<sub>3</sub> -based lead-free ceramics. *RSC Adv.* **2018**, *8*, 24286–24296. [CrossRef]

96. Zhu, F.; Skidmore, T.A.; Bell, A.J.; Comyn, T.P.; James, C.W.; Ward, M.; Milne, S.J. Diffuse dielectric behaviour in Na<sub>0.5</sub>K<sub>0.5</sub>NbO<sub>3</sub>–LiTaO<sub>3</sub>–BiScO<sub>3</sub> lead-free ceramics. *Mater. Chem. Phys.* **2011**, *129*, 411–417.. [[CrossRef](#)]
97. Panomsuwan, G.; Manuspiya, H. A comparative study of dielectric and ferroelectric properties of sol-gel-derived BaTiO<sub>3</sub> bulk ceramics with fine and coarse grains. *Appl. Phys. A* **2018**, *124*, 713. [[CrossRef](#)]
98. Li, X.; Shih, W.H. Size Effects in Barium Titanate Particles and Clusters. *J. Am. Ceram. Soc.* **1997**, *80*, 2844–2852. [[CrossRef](#)]
99. Huang, K.-C.; Huang, T.-C.; Hsieh, W.-F. Morphology-controlled synthesis of barium titanate nanostructures. *Inorg. Chem.* **2009**, *48*, 9180–9184. [[CrossRef](#)] [[PubMed](#)]
100. Maiwa, H. Piezoelectric properties of BaTiO<sub>3</sub> ceramics prepared by hot isostatic pressing. *J. Ceram. Soc. Japan* **2013**, *121*, 655–658. [[CrossRef](#)]
101. Zeinabad, H.A.; Zarabian, A.; Saboury, A.A.; Alizadeh, A.M.; Falahati, M. Interaction of single and multi wall carbon nanotubes with the biological systems: tau protein and PC12 cells as targets. *Sci. Rep.* **2016**, *6*, 26508. [[CrossRef](#)]
102. Wei, J.; Saharudin, M.S.; Vo, T.; Inam, F. N,N-Dimethylformamide (DMF) Usage in Epoxy/Graphene Nanocomposites: Problems Associated with Reaggregation. *Polymers* **2017**, *9*, 193. [[CrossRef](#)]
103. Shuai, C.; Feng, P.; Gao, C.; Shuai, X.; Xiao, T.; Peng, S. Graphene oxide reinforced poly(vinyl alcohol): Nanocomposite scaffolds for tissue engineering applications. *J. RSC Adv.* **2015**, *5*, 25416–25423. [[CrossRef](#)]
104. Cui, C.; Baughman, R.H.; Iqbal, Z.; Kazmar, T.R.; Dahlstrom K. Piezoelectrics and Related Devices from Ceramics Dispersed in Polymers, U.S. Patent US5951908A, 14 September 1999.
105. Payo, I.; Hale, J.M. Dynamic characterization of piezoelectric paint sensors under biaxial strain. *Sens. Actuators A Phys.* **2010**, *163*, 150–158. [[CrossRef](#)]
106. Kok, S.L.; Lau, K.-T.; Ahsan, Q. Substrate-Free Thick-Film Lead Zirconate Titanate (PZT) Performance Measurement Using Berlincourt Method. *Adv. Mater. Res.* **2014**, *895*, 204–210. [[CrossRef](#)]
107. Gentry, S.P.; Halloran, J.W. Depth and width of cured lines in photopolymerizable ceramic suspensions. *J. Eur. Ceram. Soc.* **2013**, *33*, 1981–1988. [[CrossRef](#)]
108. Chabok, H.; Zhou, C.; Chen, Y.; Eskandarinazhad, A.; Zhou, Q.; Shung, K. Ultrasound Transducer Array Fabrication Based on Additive Manufacturing of Piezocomposites. In Proceedings of ASME/ISCIIE 2012 International Symposium 2012, St. Louis, MI, USA, 18–20 June 2012; pp. 433–444. [[CrossRef](#)]
109. Azan, V.; Lecamp, L.; Lebaudy, P.; Bunel, C. Simulation of the photopolymerization gradient inside a pigmented coating. *Prog. Org. Coat.* **2007**, *58*, 70–75. [[CrossRef](#)]
110. Dang, Z.-M.; Fan, L.-Z.; Shen, Y.; Nan, C.-W. Dielectric behavior of novel three-phase MWNTs/BaTiO<sub>3</sub>/PVDF composites. *Mater. Sci. Eng. B* **2003**, *103*, 140–144. [[CrossRef](#)]
111. Babu, I.; de With, G. Enhanced electromechanical properties of piezoelectric thin flexible films. *Compos. Sci. Technol.* **2014**, *104*, 74–80. [[CrossRef](#)]
112. Guan, X.; Zhang, Y.; Li, H.; Ou, J. PZT/PVDF composites doped with carbon nanotubes. *Sens. Actuators A Phys.* **2013**, *194*, 228–231. [[CrossRef](#)]
113. Liu, X.F.; Xiong, C.X.; Sun, H.J.; Dong, L.J.; Li, R.; Liu, Y. Piezoelectric and dielectric properties of PZT/PVC and graphite doped with PZT/PVC composites. *Mater. Sci. Eng. B* **2006**, *127*, 261–266. [[CrossRef](#)]
114. Banerjee, S.; Du, W.; Sundar, U.; Cook-Chennault, K.A. Piezoelectric and Dielectric Characterization of MWCNT-Based Nanocomposite Flexible Films. *J. Nanomater.* **2018**, *2018*, 6939621. [[CrossRef](#)]
115. Banerjee, S.; Cook-Chennault, K.A.; Du, W.; Sundar, U.; Halim, H.; Tang, A. Piezoelectric and dielectric characterization of corona and contact poled PZT-epoxy-MWCNT bulk composites. *Smart Mater. Struct.* **2016**, *25*, 115018. [[CrossRef](#)]
116. Granzow, T.; Kounga, A.B.; Aulbach, E.; Rödel, J. Electromechanical poling of piezoelectrics. *Appl. Phys. Lett.* **2006**, *88*, 252907. [[CrossRef](#)]
117. Wu, J.; Xiao, D.; Wu, W.; Chen, Q.; Zhu, J.; Yang, Z.; Wang, J. Composition and poling condition-induced electrical behavior of (Ba<sub>0.85</sub>Ca<sub>0.15</sub>)(Ti<sub>1-x</sub>Zr<sub>x</sub>)O<sub>3</sub> lead-free piezoelectric ceramics. *J. Eur. Ceram. Soc.* **2012**, *32*, 891–898. [[CrossRef](#)]
118. Du, H.; Tang, F.; Luo, F.; Zhou, W.; Qu, S.; Pei, Z. Effect of poling condition on piezoelectric properties of (K<sub>0.5</sub>Na<sub>0.5</sub>)NbO<sub>3</sub>–LiNbO<sub>3</sub> lead-free piezoelectric ceramics. *Mater. Sci. Eng. B* **2007**, *137*, 175–179. [[CrossRef](#)]
119. Egusa, S.; Iwasawa, N. Piezoelectric paints as one approach to smart structural materials with health-monitoring capabilities. *Smart Mater. Struct.* **1998**, *7*, 438–445. [[CrossRef](#)]
120. Egusa, S.; Iwasawa, N. Piezoelectric paints: Preparation and application as built-in vibration sensors of structural materials. *J. Mater. Sci.* **1993**, *28*, 1667–1672. [[CrossRef](#)]
121. Payo, I.; Hale, J.M. Sensitivity analysis of piezoelectric paint sensors made up of PZT ceramic powder and water-based acrylic polymer. *Sens. Actuators A Phys.* **2011**, *168*, 77–89. [[CrossRef](#)]
122. Umemura, N.; Yoshida, K.; Kato, K. Phase-matching properties of KNbO<sub>3</sub> in the mid-infrared. *Appl. Opt.* **1999**, *38*, 991–994. [[CrossRef](#)]
123. Karvounis, A.; Timpu, F.; Vogler-Neuling, V.V.; Savo, R.; Grange, R. Barium Titanate Nanostructures and Thin Films for Photonics. *Adv. Opt. Mater.* **2020**, *8*, 2001249. [[CrossRef](#)]

124. Wemple, S.H.; Didomenico, M.; Camlibel, I. Dielectric and optical properties of melt-grown BaTiO<sub>3</sub>. *J. Phys. Chem. Solids* **1968**, *29*, 1797–1803. [[CrossRef](#)]
125. Müller, M.T.; Hilarius, K.; Liebscher, M.; Lellinger, D.; Alig, I.; Pötschke, P. Effect of Graphite Nanoplate Morphology on the Dispersion and Physical Properties of Polycarbonate Based Composites. *Materials* **2017**, *10*, 545. [[CrossRef](#)]

**Disclaimer/Publisher's Note:** The statements, opinions and data contained in all publications are solely those of the individual author(s) and contributor(s) and not of MDPI and/or the editor(s). MDPI and/or the editor(s) disclaim responsibility for any injury to people or property resulting from any ideas, methods, instructions or products referred to in the content.